Master's Thesis

석사 학위논문

Experimental Study on the Degradation Mechanisms of Proton Exchange Membrane Fuel Cells Using the Accelerated Stress Test Method

Sangheum Byun(변 상 흠 卞 相 欽)

Department of Energy Systems Engineering

에너지시스템공학전공

DGIST

2014

Master's Thesis

석사 학위논문

Experimental Study on the Degradation Mechanisms of Proton Exchange Membrane Fuel Cells Using the Accelerated Stress Test Method

Sangheum Byun(변 상 흠 卞 相 欽)

Department of Energy Systems Engineering

에너지시스템공학전공

DGIST

2014

Experimental Study on the Degradation Mechanisms of Proton Exchange Membrane Fuel Cells Using the Accelerated Stress Test Method

Advisor: Professor   Byungchan Han

Co-advisor: Doctor   Young-Gi Yoon

by

Sangheum Byun

Department of Energy Systems Engineering

DGIST

A thesis submitted to the faculty of DGIST in partial fulfillment of the requirements for the degree of Master of Science in the Department of Energy Systems Engineering. The study was conducted in accordance with Code of Research Ethics[1].

06. 09. 2014

Approved by

Professor Byungchan Han   _____
(Advisor)

Doctor Young-Gi Yoon   _____
(Co-Advisor)

---

[1] Declaration of Ethical Conduct in Research: I, as a graduate student of DGIST, hereby declare that I have not committed any acts that may damage the credibility of my research. These include, but are not limited to: falsification, thesis written by someone else, distortion of research findings or plagiarism. I affirm that my thesis contains honest conclusions based on my own careful research under the guidance of my thesis advisor.

Experimental Study on the Degradation Mechanisms of Proton Exchange Membrane Fuel Cells Using the Accelerated Stress Test Method

Sangheum Byun

Accepted in partial fulfillment of the requirements for the degree of
Master of Science.

06. 09. 2014

Head of Committee   Byungchan Han   (인)

한병찬 교수

Committee Member   Young-Gi Yoon   (인)

윤영기 박사

Committee Member Sangaraju Shanmugam(인)

샹가라쥬 샨무감 교수

MS/ES
201224014

변 상 흠. Sangheum Byun. Experimental Study on the Degradation Mechanisms of Proton Exchange Membrane Fuel Cells Using the Accelerated Stress Test Method. Department of Energy Systems Engineering. 2014. 39P. Advisor Prof. Byungchan Han, and Co-Advisor Dr. Young-Gi Yoon.

Abstract

Long-term durability of a Polymer Electrolyte Membrane Fuel Cell (PEMFC) is the main bottleneck to a wide-scale of commercialization for the power sources of various devices. Over the last several decades focused researches have been conducted to investigate its mechanism but still isolated facts and mechanisms have been found. In this thesis, in-situ electrochemical measurements and scanning electron microscope (SEM) which belongs to ex-situ measurement were conducted to investigate the systematic analysis for degradation mechanisms of PEMFC under three modes of Accelerated Stress Test (AST) methods. The objectives of the thesis are to determine the causes of degradations and mechanisms by identifying microstructural changes in the PEMFC especially in MEA. To achieve the goals, we made the MEA and prepare other components of PEMFC to setup the PEMFC single cell system. Three different modes of AST were applied to study degradation behaviors in fast time. Polarization curve, high frequency resistance (HFR) and cyclic voltammetry (CV) were conducted to estimate the changes of performance of cell which indicates the whole reaction rate of single cell, the contacts between the components of MEA and electrochemical surface area (ECSA) which indicates the active Pt surface area. Activation overvoltage and the Tafel slope take a role to

identify degradation mechanism related to characteristics of Pt. Limiting current density and contribution of mass transport overvoltage feeding low concentration reactants show the direct trends of mass transport of reactants. Our results indicate that the collapse of carbon support and the subsequent local environment which surrounds carbon support is the major factors controlling the long-term durability of a PEMFC at AST on carbon support materials. Contact loss of ionomer with support and catalyst degradation simultaneously occur at AST on catalyst materials. With relatively high temperature and low relative humidity (RH) conditions, pinhole formations may be the reason of membrane/ionomer degradation.

Contents

List of figures

List of tables

Chapter 1

Introduction

1.1 Introduction of PEM fuel cells

The rapid growth of human population and desire for using high quality of modern technology have ever increased fossil-fuel based energy consumption inducing significant depletion of natural resources and environmental degradation.[1].

A Polymer Electrolyte Membrane Fuel Cell (PEMFC) has been considered as an alternative device harvesting renewable energies[2] since it does not produce any environmental pollutants such as nitrogen oxide (NOx), sulfur oxide (SOx), carbon dioxide (CO_2), and so on. In addition, it is much more efficient[3] in generation of electricity than conventional internal combustion engines.

A PEMFC mainly composed of six components: membrane, catalyst layer (CL), gas diffusion layer (GDL), bipolar plate, current collecting plate and end plate as shown at Fig. 1.1. The working principle of the PEMFC is that the fuels H_2 and O_2 gases are fed to anode and cathode, respectively to produce electricity by electrochemically forming water as described at eq. (1), (2) and (3) [4],

$$\text{Anode (hydrogen oxidation reaction, HOR): } H_2 \rightarrow 2H^+ + 2e^- \qquad (1)$$

$$\text{Cathode (oxygen reduction reaction, ORR): } \frac{1}{2}O_2 + 2H^+ + 2e^- \rightarrow H_2O \qquad (2)$$

$$\text{Overall reaction: } H_2 + \frac{1}{2}O_2 \rightarrow H_2O \ (E^0 \cong 1.23 \text{ V vs. SHE}) \qquad (3)$$
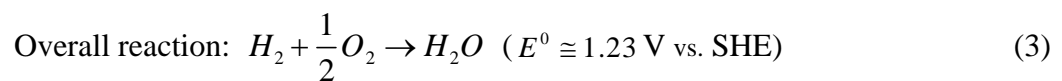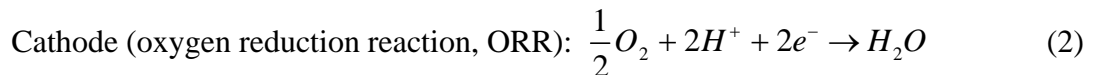
where, E^0 is thermodynamic equilibrium potential in aqueous solution at $25\,^\circ\mathrm{C}$, 1 atm. These reactions occur at membrane electrode assembly (MEA) consisting of membrane, two electrodes and Gas Diffusion Layer (GDL). The GDL is an electronic conductor permitting diffusion of fuel gases into the interfaces of the catalyst and the membrane and transporting liquid water to the gas flow channels. At the surface of anode catalyst layer, gas phase H_2 molecules are electrochemically oxidized into proton (H^+) and electrons. While electrons travel through the external electric circuit protons diffuse into cathode electrode through the membrane. Protons drag one or several water molecules (an electro-osmotic drag[5]) when they diffuse through the membrane (Nafion[6,7]). At the cathode, oxygen gas reduces into O^{2-} (Oxygen Reduction Reaction, ORR) by electrocatalysts and then, reacts with the protons transported through the membrane to form water. Thus, O^{2-} ,H^+ and electrons meet at a triple phase boundary (TPB) as shown at Fig.1.

The main issues for the commercialization of PEMFCs are three part: Low catalytic activity toward ORR, High material cost and weak durability. The durability is still far off DOE targets (by 2020, improve durability to 5,000 hours, which is equivalent to 150,000 miles of driving but recent reports show that the lifetime of PEMFC vehicles is 1700h and 2000h[8,9] ,and lifetime of a fuel cell is assessed by the number of hours until 10% power is lost)[10,11]. Generally speaking, securing the long-term stability is an essential for the power sources of electric vehicles and residential areas. As such to understand fundamental degradation mechanisms is of importance to design the high functional PEMFC devices.

There are several factors which causes complex degradation mixed with each other, and especially for automobile use, dynamic driving conditions of automobile makes it easier to degrade than stationary PEMFC facilities.

Until now degradation of components of PEMFC have been investigated but papers dealing with analysis of microstructures of PEMFC are relatively little, and even disagreements for the cause or mechanisms of PEMFC have been found. Moreover, systematic quantification and analysis of causes for PEMFC degradation are very few.

Accelerated stress test (AST) methods[12,13] are widely used to study such degradation behaviors in reasonably fast time scale. Borup et al. propose five different parameters in accelerated stress tests (ASTs)[14]: temperature of cell, relative humidity 3) operating voltage, 4) open circuit voltage (OCV) and 5) cycling (relative humidity, temperature, voltage, freeze/thaw, or start/stop) parameters. And these several parameters possibly makes the similar situations of degradations of PEMFC which powers automobiles.

In this thesis, AST methods were performed to investigate detailed mechanisms and causes of PEMFC durability degradation with varying conditions of : 1) 65℃, RH 100 %, 1.4 V voltage hold, 2) 80℃, RH 100 %, voltage cycling (0.6 - 1.0 V) and 3) 90℃, RH 10 %, and OCV hold. And also we use systematic approaches for elucidate the mechanisms and the cause of degradations of PEMFC.
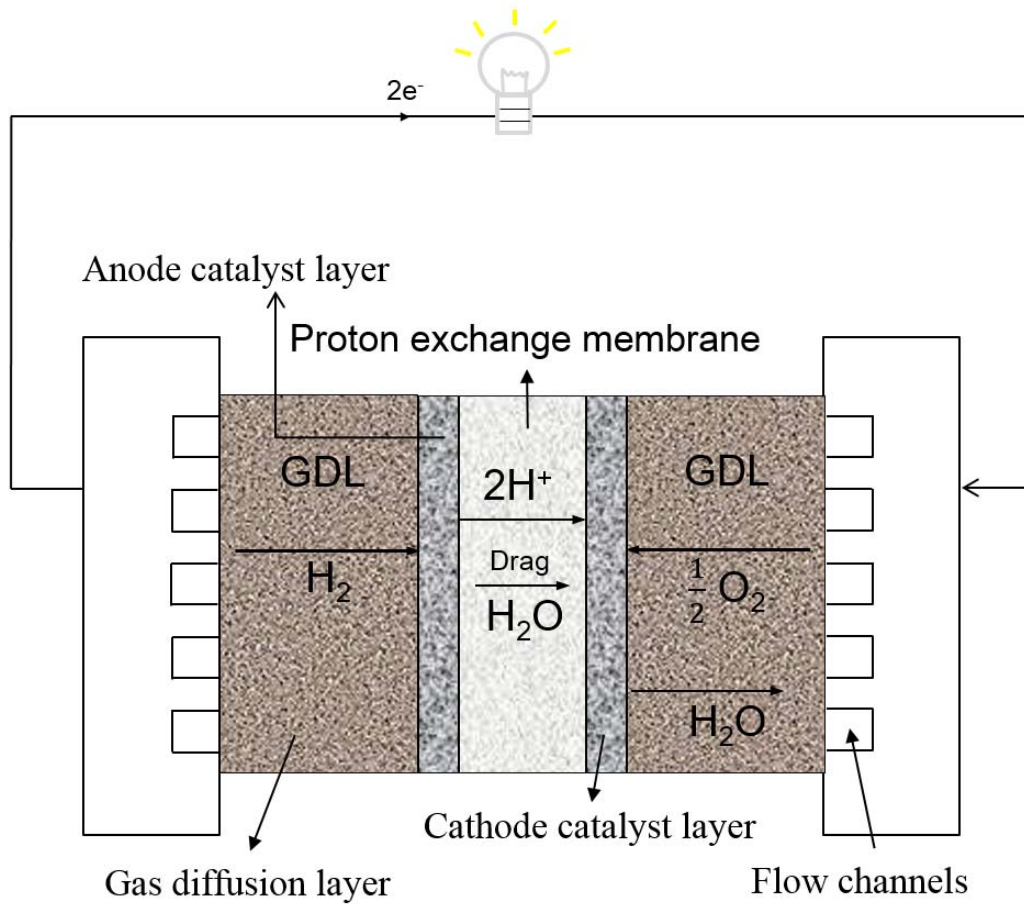
Figure 1.1 Schematic diagram of a PEM fuel cell configuration, showing components and operating mechanism.

Figure 1.2 Simplified and idealized structure of a PEM fuel cell electrode[15].

1.2 Objective of thesis

Various in-situ electrochemical experiments and SEM which belongs to ex-situ experiment for single cell ($1.5cm^2$) were used to investigate causes of degradation and estimate changes of components of PEMFC in this thesis.

(1) Several in-situ electrochemical measurements and ex-situ method, SEM, was conducted: from the measurements of limiting current density[5] which is determined by supply of proton, oxygen and electrons (usually there are no transport limitations of electrons except short circuit) and overpotentials were evaluated to understand mechanisms of the degradation of PEMFC.

(2) Agglomerate CCL model [16-18] was utilized to explain our experimental results, which decouple only the contribution of CCL from the total degradations. Limiting current density was measured to characterize the CCL structures over the PEMFC operation.

(3) Based on our study it is proposed how to enhance the durability of a PEMFC system.

Chapter 2

Experimental

2.1 Preparation of MEA & components

Catalyst ink for both sides of the electrodes was prepared by mixing Pt/C powder (3g, 40 wt %

with Nafion 212 solution (28.5g, 5 wt % Nafion 212, Dupont) and solvent (with platinum

loading 0.31, 0.27 mg_{Pt}/cm^2). magnetic stirrer used to well disperse catalyst ink. It was coated

with following procedures: a roll-to-roll process is used by applying the doctor blade method

and then the electrocatalysts which become catalyst layers are hot pressed at 140℃ on Nafion

212 by the decal method.

The membrane electrode assembly (MEA) of an active area 1.5 cm^2 was assembled with

sealing gasket, gas diffusion layers (GDL, 10 BC), graphite bipolar plates with a serpentine gas

channel, gold-coated current collecting plates and end plates.

2.2 Electrochemical measurements

All electrochemical measurements were carried out in a single cell at temperature 65 ℃ with

fully humidified (RH 100 %) gas conditions. The cell performance was evaluated using a fuel

cell automated test system (FCATS) G20 (Green-Light innovation, Vancouver, Canada). All

electrochemical measurements were conducted using Bio-logic HCP – 803 with their built-in

programmed electrochemical techniques. We put 2 lpm at the anode and 3 lpm at the cathode,

and the anode feeding H_2/N_2 ratio and cathode feeding O_2/N_2 ratio were adjusted during the

measurements of polarization curve, high frequency resistance (HFR), and Tafel slope. Polarization technique was applied to measure fuel cell performance under fully humidified reactants. Potentiostatic measurements from 0.8 V to 0.3 V with 0.05 V declination in case of H_2/air each sides, and these of from 0.8 V to 0.2 V with 0.05 V declination in case of H_2 3, 4, 5%/air and H_2/O_2 2, 4, 6% were conducted under 2, 3 lpm at anode and cathode. HFR was measured within each steps of polarization measurements using the EIS potentiostat in the frequency range of 100 ~ 1 kHz with 12 points/decade. Tafel slope was performed to measure the activation overpotentials with condition of 1 mV/s scan rate. The cyclic voltammetry (CV), linear sweep voltammetry (LSV) were conducted with 2 nlpm of H_2/N_2. The CVs were measured for investigating the electrochemical active surface area (ECSA) of the cathode catalyst layer (CCL) with a scan rate of 100 mV/s and potential from 0.01 V to 1.2 V (vs. SHE), and both sides of 2 lpm. The ECSA of Pt in the CCL was determined from an H-desorption charge with an assumption of 210 $\mu C/cm_{Pt}{}^2$ for Pt surface area. LSV technique was conducted to measure the hydrogen crossover rate (in mA/cm^2) with voltage ranges from 0.2 V to 0.6 V while supplying 2 lpm of H_2/N_2.

2.3 Accelerated stress test

Three modes of accelerated stress tests (ASTs) were conducted in this thesis. Carbon support degradation was performed by holding potential for 15 h at 1.4 V in condition of cell temperature 65 ℃, fully humidified RH with 2 lpm of H_2/N_2. (called as support AST) Within each 5 hour, the electrochemical measurements and AST were sequentially conducted starting with the initial electrochemical measurements. Catalyst degradation was performed by using

linear sweep in voltage from 0.6 V to 1.0 V with 100 mV/s in condition of cell temperature 80 ^{o}C, fully humidified RH with 2 lpm of H_2/N_2,[19] and 60,000 cycles of degradation of the degradation were applied (called as catalyst AST). At every single set of 20,000 cycles (consists of three sets) electrochemical measurements were conducted at 65℃, fully humidified condition to identify any change in the cell performances. Membrane/ionomer degradation was performed by holding OCV for 60 h at 90 ℃, RH 10 % at both electrode (DP - 39.2 ℃) with H_2/air 2, 3 lpm (called as membrane/ionomer AST). Within every 20 h, electrochemical measurements were performed. Figure 2.1 represents overall scheme of the experimental procedures.

The initial Electrochemical measurements
↓
1st AST
↓
1st Electrochemical measurements
↓
2nd AST
↓
2nd Electrochemical measurements
↓
3rd AST
↓
3rd Electrochemical measurements

Experimental procedure

Cyclic voltammetry 0.01 – 1.2 V potential sweep with H_2/N_2
↓
Hydrogen permeation 0.2 V – 0.6V Linear sweep voltammetry with H_2/N_2
↓
Polarization curve + HFR 0.3 V – 0.8 V (including OCV measure) with H_2/air
↓
Polarization curve + HFR 0.2 V – 0.8 V (including OCV measure) with H_2/O_2 (2,4,6%) and H_2 (3,4,5%)/air
↓
Tafel slope Potential sweep (1 mV/s scan rate) with H_2/O_2 (2,4,6%) and H_2 (3,4,5%)/air

Electrochemical measurements

Figure 2.1 flow chart of experimental procedure and Electrochemical measurements.

2.4 Structural characterization of MEA by SEM

Characteristics of MEA were measured by ex-situ post-mortem measurements. Cross-section observations of the MEAs, which were prepared by freezing the sample in liquid nitrogen and fracturing it, were analyzed with a scanning electron microscope (SEM)[20,21]. The results provided information of the thicknesses of cross-sections of MEAs of the initial state as well as that of fully degraded state by the AST methods.

Chapter 3

Results and discussion

3.1 Microstructural changes of MEA under AST on catalyst materials

Catalyst AST is the process which mainly cause catalyst degradation with voltage sweep from 0.6 V to 1.0 V for scan rate of 100 mV/s and cell temperature 80℃. Reduction of CCL thickness and loss of ECSA caused by Pt catalyst degradation have been reported while catalyst degradation proceed[22]. Even though carbon corrosion occurs at 0.207 V (vs. SHE)[23] kinetics of corrosion is slow enough under 1.0 V[12,24] that we can possibly think the catalyst degradation as a main factor.

Polarization curves and HFRs were shown in figure 3.1. Among low hydrogen and oxygen cases, H_2 4%/air and H_2/O_2 4% were selected as representatives. HFRs were almost same as the AST proceed, and it means that no significant contact loss between carbon supports. We also expect no changes of connectivity and characteristics of ionomer in CCL through which proton transport. Limiting current density losses ranged over 0 - 17% in all reactant cases, which were relatively small compared with that of AST on support degradation, and performance losses were shown.

ECSA derived from CV technique was decreased 76% after 60000 cycles AST while performance and Limiting current densities almost remained at H_2 (3, 4, 5 %)/air. We measured CV, Tafel slope, activation overvoltage, contribution of mass transport overvoltage and limiting current density analysis under catalyst AST to identify whether catalyst degradation only affect to losses of Pt catalyst surface area or changes of activity of Pt catalyst. Tafel slopes show almost no change at all conditions with AST time in figure 3.2. This means that catalyst itself

and local environments which surround catalyst have no changes. Figure 3.3 shows that experimental increment of overvoltage values are 25-31 mV which is relatively smaller than theoretical value while theoretical increment of activation overvoltages are about 60 mV when Pt ECSA decreases 76% from the initial. It means that loss of Pt surface area is not the main reason of catalyst degradation. Pt catalyst corrosion rate under the AST on the catalyst degradation is different from each facets, and there are references that high catalytic activity facets remain more than others which have low activities[25,26]. This reports support our experiment by compensating the differences between experimental and theoretical increment of overvoltage.

Catalyst corrosion progress known as: after Pt oxidation occurs, Pt catalyst dissolved as Pt ion (mostly Pt^{2+}). Hydrogen permeation current was about 11 mA/cm^2, which makes hydrogen possibly transport through membrane to cathode. Permeated hydrogen gas is expected to precipitate Pt ions into Pt agglomerates, and significant amount of precipitated Pt is expected to be found in the membrane and ionomer in CCL under the condition of high hydrogen permeation current and loss of Pt ECSA[12]. These Pt precipitations in the membrane and ionomer in CCL may affect to proton conductivity of MEA. but in our experiments limiting current density almost remained at H_2 (3, 4, 5 %)/air, and it means that precipitated Pt does not affect characteristics of proton conductivity.

(a) Polarization curves at H₂/air

(b) Polarization curves at H₂ 4%/air

(c) Polarization curves at H₂/O₂ 4%
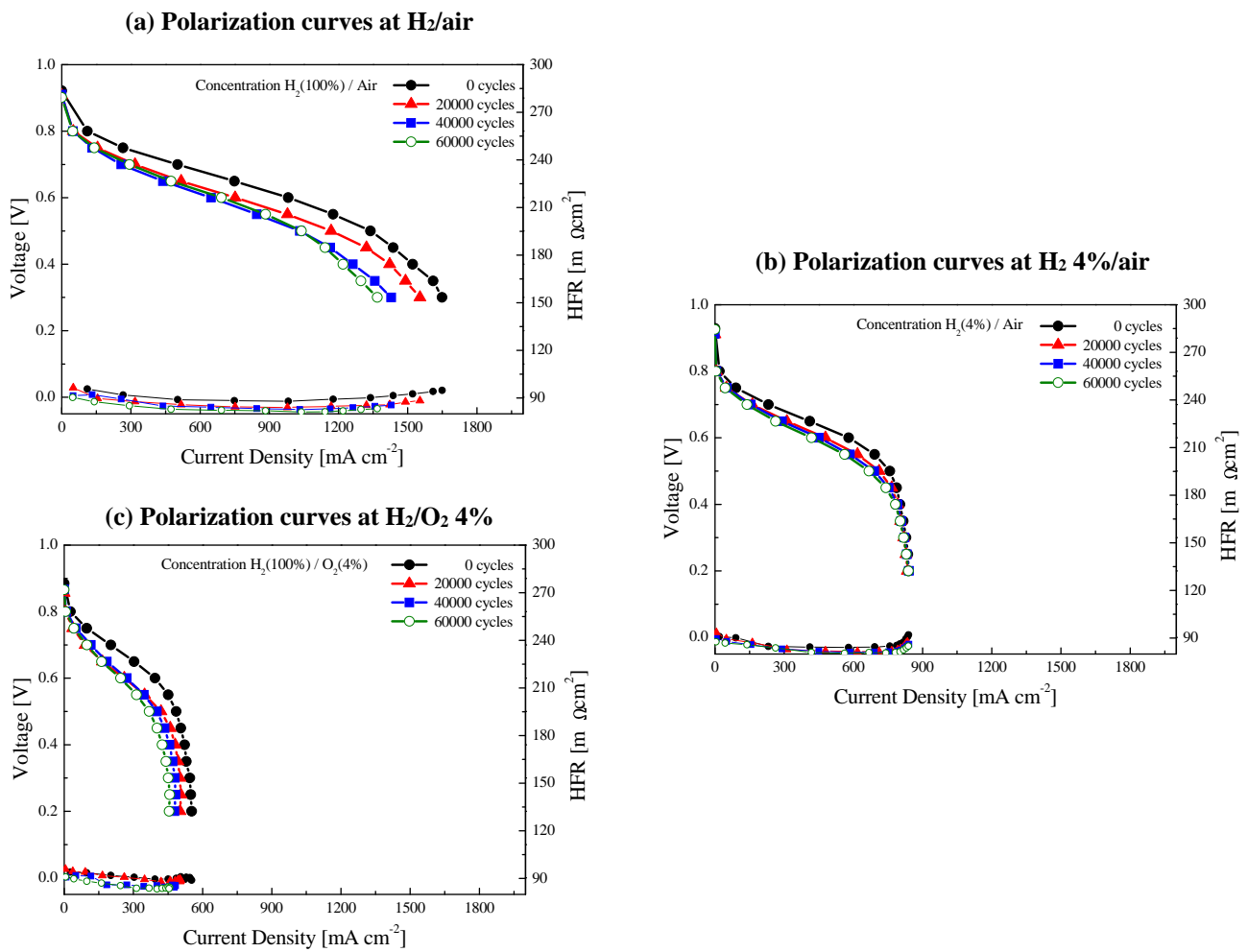
Figure 3.1 The polarization curves and HFRs of H₂/air, H₂ 4%/air and H₂/O₂ 4% are indicated in (a), (b) and (c) respectively against current density. Each symbols in the figures represent polarization curve with each 20000 cycles of AST for condition of An 2 lpm/Ca 3 lpm, cell temperature of 65℃ and RH 100%. Polarization curves in (a), (b) and (c) decrease with AST time while HFR values remain almost constant.

(a) Tafel slope against catalyst AST time at H₂/air and H₂ (3, 4, 5 %)/air
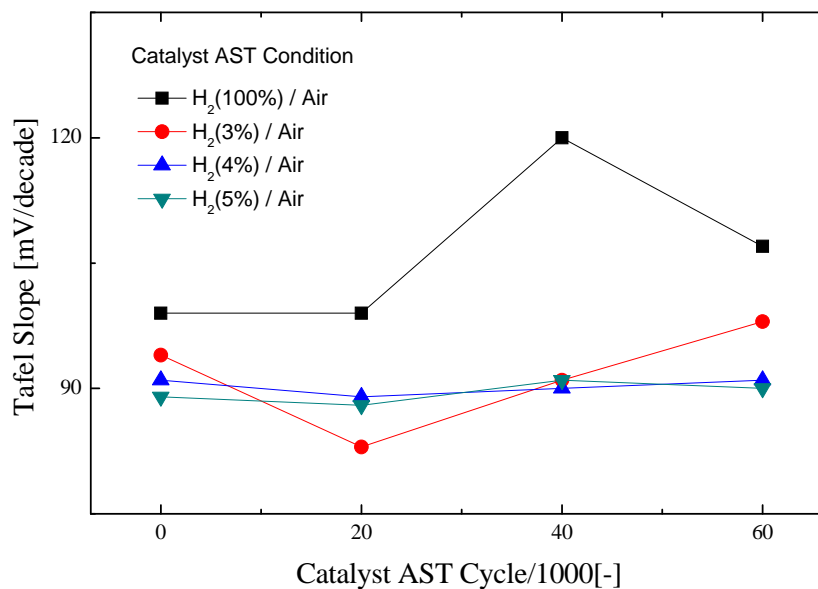
(b) Tafel slope against catalyst AST time at H₂/air and H₂/O₂ (2, 4, 6 %)
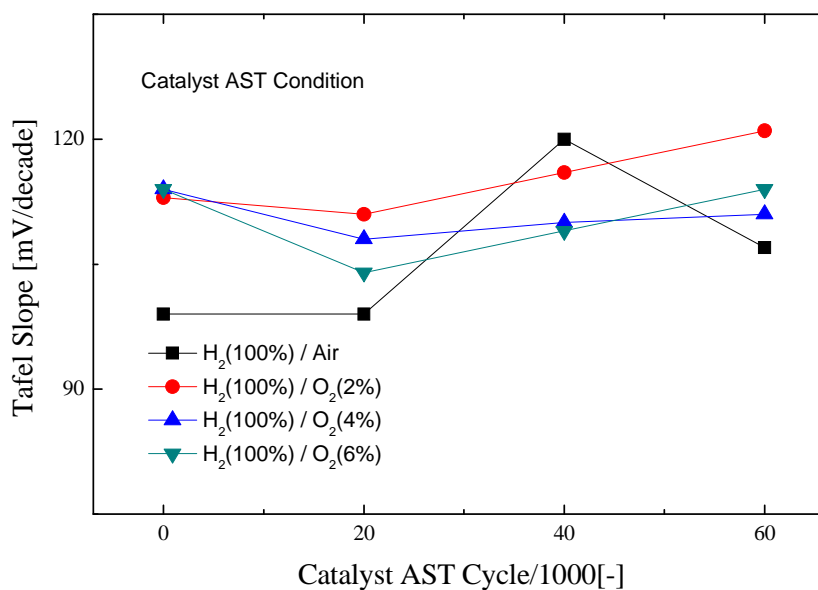
Figure 3.2 Tafel slopes against catalyst AST plotted with reactatants of (a) H₂/air and H₂ (3, 4, 5%)/air and (b) H₂/air and H₂/O₂ (2, 4, 6%).

(a) Activation overvoltage at H₂/air

(b) Activation overvoltage at hydrogen (H₂ 3, 4, 5%)/air

(c) Activation overvoltage at H₂/oxygen (O₂ 2, 4, 6%)
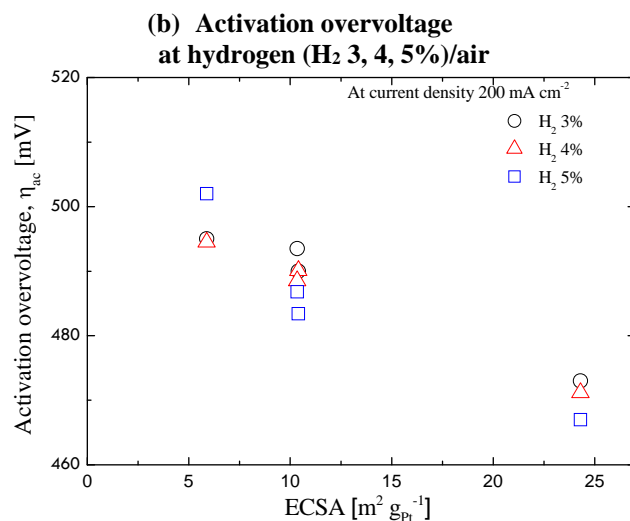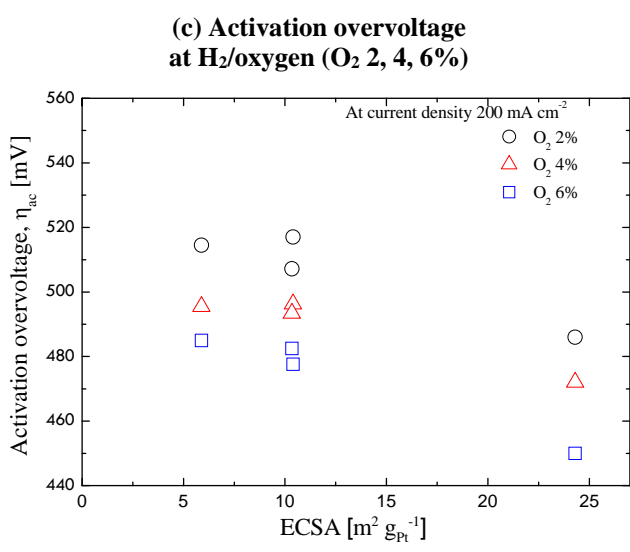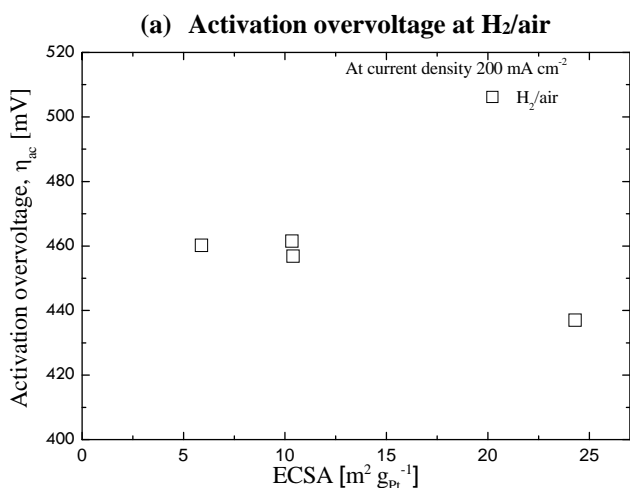
Figure 3.3 Activation overvoltage against ECSA under catalyst AST. Activation overvoltage of H₂/air, H₂ (3, 4, 5%)/air and H₂/O₂ (2, 4, 6%) are indicated in (a), (b) and (c) respectively against ECSA. Each symbols in the figures represent activation overvoltage with each reactant concentration for condition of An 2 lpm/Ca 3 lpm, cell temperature of 65℃ and RH 100%.

14

(a) Contribution of mass transport overvoltage at H₂/air
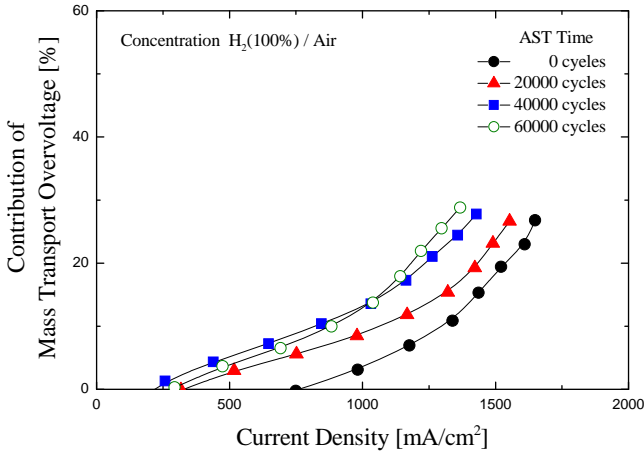
(b) Contribution of mass transport overvoltage at H₂ 4%/air
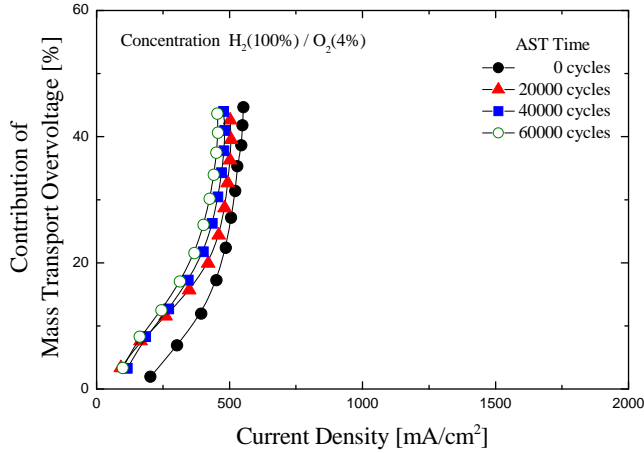
(c) Contribution of mass transport overvoltage at H₂/O₂ 4%
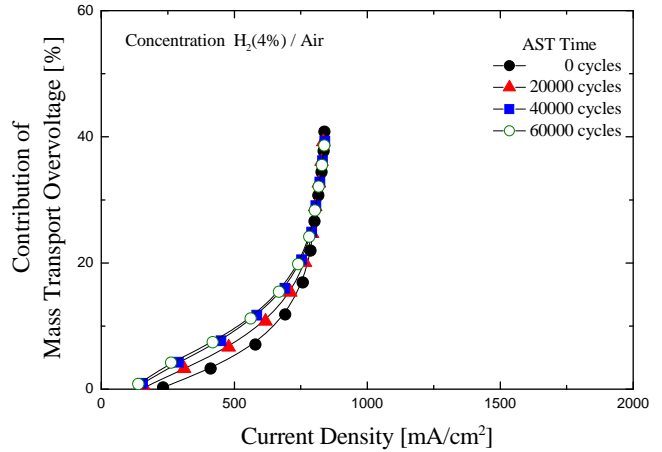
Figure 3.4 Contribution of Diffusion Overvoltages as a function of the current density with each symbols represents respectively states between 20000 cycles of catalyst AST process at (a) H₂/air, (b) H₂ 4%/air and (c) H₂/O₂ 4% feed conditions of An 2 lpm/Ca 3 lpm, cell temperature of 65℃ and RH 100%.

To summarize results of our experimental data, even though Pt ECSA decreased ratio of higher activity Pt catalyst facets increased so performance loss was not big. Corrosion of Pt has almost no effects on the characteristics of proton conductivity of membrane and ionomer in CCL. Also connectivity between carbon support was almost no damaged. Following figure 3.5 shows the

systematic analysis on the identifying cause of degradation under catalyst AST.
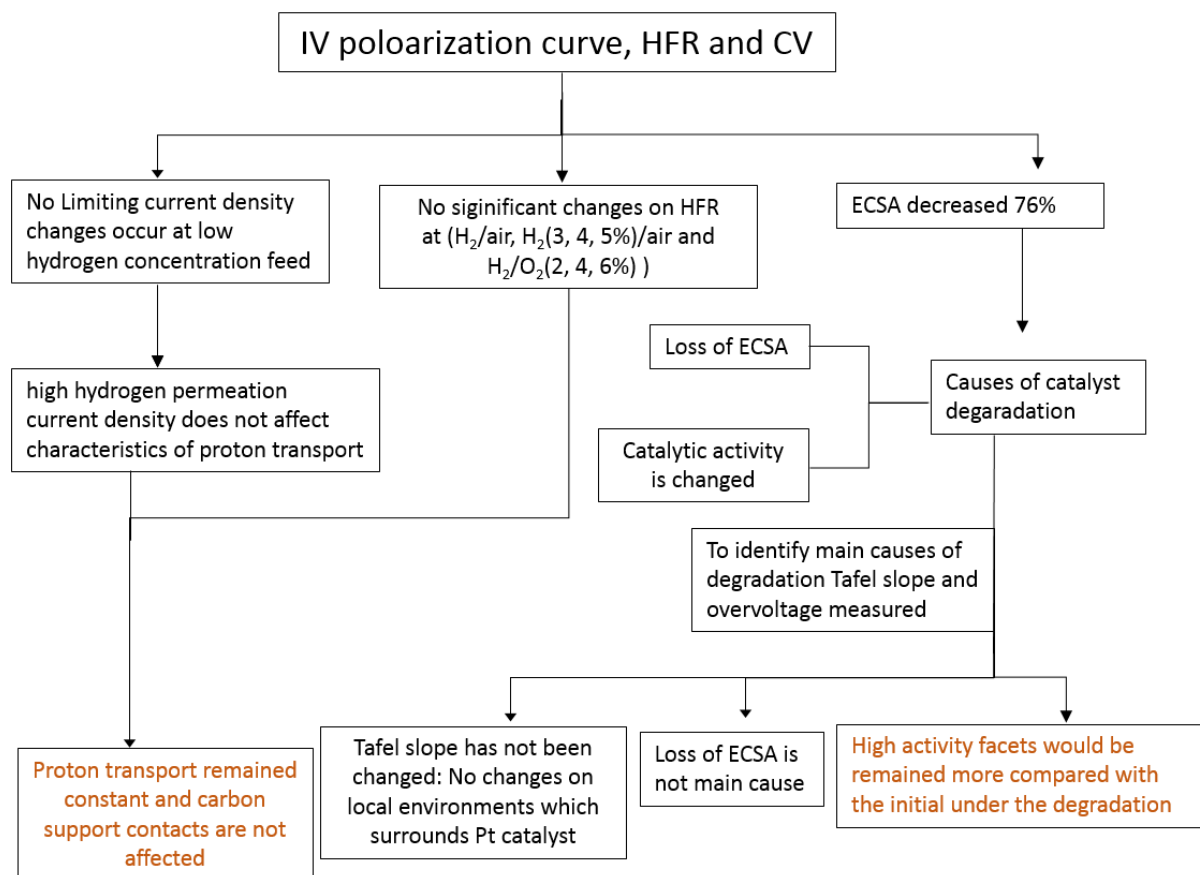
Figure 3.5 Systematic analysis scheme of degradation under AST on catalyst materials.

3.2 Microstructural changes of MEA under AST on support materials

Support AST is the process which mainly cause support materials degradations with high voltage hold at 1.4 V[12,27]. In the process, CCL thickness was reduced implying there is a loss of carbon support materials. Then, the HFR may increase due to raised contact resistance between carbon support and the catalyst layers. Then, the HFR may increase due to increase of contact resistance of carbon support[27]. To accurately identifying whether support degradation causes loss of catalyst layer thickness and contact loss or affects state of ionomer and activity

of catalyst, electrochemical measurements were conducted.

Polarization curves and HFRs were shown in figure 3.6 to investigate the changes of unit cell performance, limiting current density and contacts of components of cell. Limiting current density losses ranged over 25 - 50% in all feeding cases. ECSA derived from CV measurement indicates 72 % decreased. Increase of HFR indicates the contacts of carbon support and membrane/ionomer individually and also the contacts between carbon support and membrane/ionomer.

To find other effects of degradation except loss of carbon supports, Tafel slope and activation overvoltages versus ECSA were analyzed to investigate catalytic effect on the degradation of PEMFC. Tafel slope was plotted by iR-corrected voltage against logarithm of current density of cell from which hydrogen permeation current density subtracted. Figure 3.7 shows that Tafel slopes were increased about 50 mV/decade, 30 mV/decade and 70 mV/decade at H_2/air, H_2 (3, 4, 5 %)/air and H_2/O_2 (2, 4, 6 %) respectively with AST time. These indicate that Pt catalyst and its local environment which surround Pt catalyst were significantly changed. Tafel slope depends on (1) Pt catalyst crystal facet, (2) oxidation state of Pt surface and (3) characteristics of electrolyte which surround Pt particle. Ratio of crystal facets of Pt affects the Tafel slope[28] but it is not sufficient to explain[29] the significant changes in Tafel slopes from 110 mV/decade to 180 mV/decade at H_2/O_2 4%. Figure 3.8 shows that the activation overvoltage increased about 60 – 70 mV, which is similar to theoretical prediction[12] of 65 mV when Pt catalyst surface decreased by 72%. This shows that contribution of oxide formation on overvoltage is not significant by describing cause of increase of activation overvoltage as catalyst loss. Local environment surrounding Pt catalyst seems to be the main cause of increase of Tafel slope according to changes of Tafel slope and activation overvoltages after degradation.

(a) Polarization curves at H₂/air

(c) Polarization curves at H₂/O₂ 4%

(b) Polarization curves at H₂ 4%/air
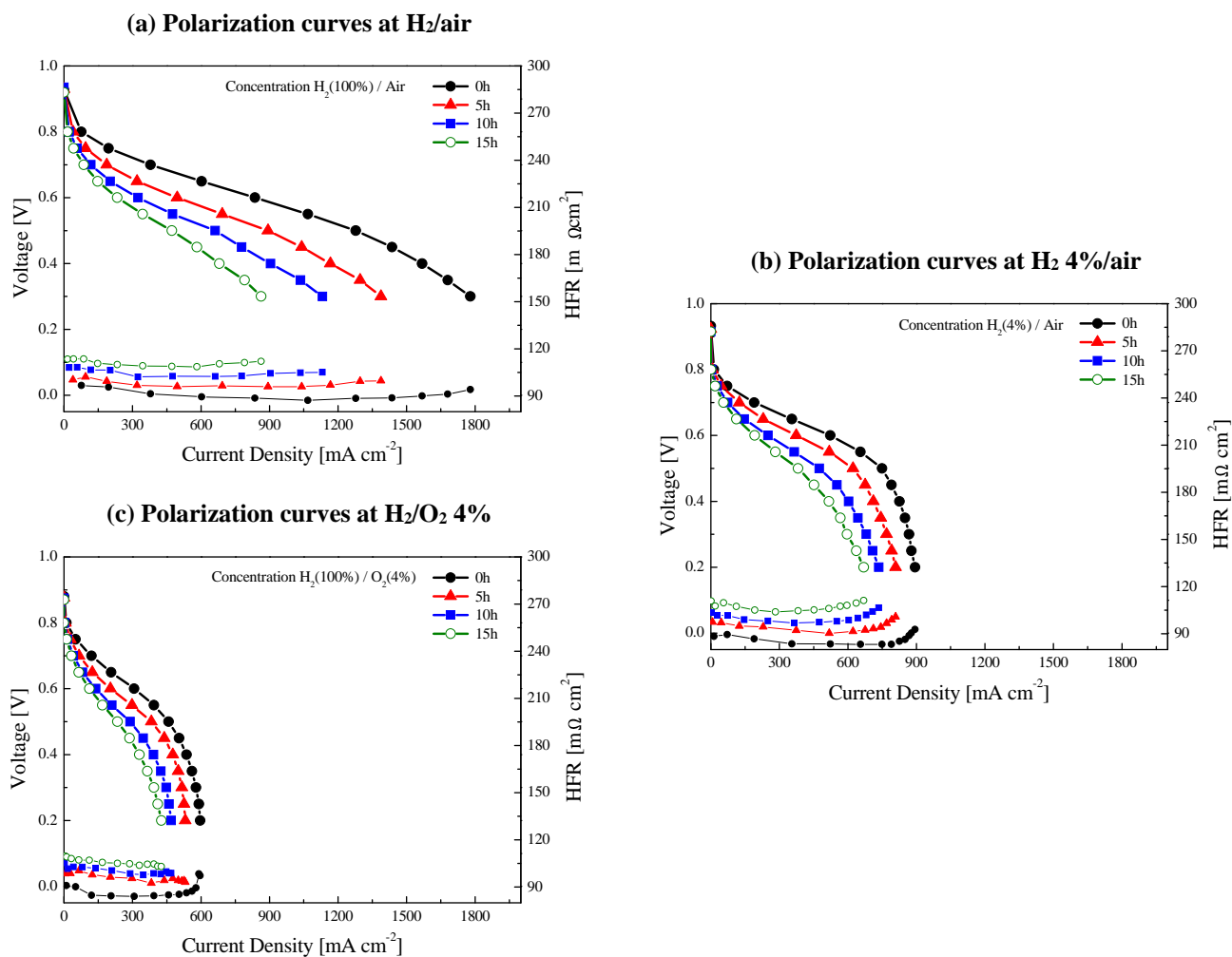
Figure 3.6 The polarization curves and HFR of H₂/air, H₂ 4%/air and H₂/O₂ 4% against current density were indicated in (a), (b) and (c) respectively under support AST. Each lines in the figures represents polarization curve with each 5 h of AST for condition of An 2 lpm/Ca 3 lpm, cell temperature of 65 ℃ and RH 100 %.

(a) Tafel slope against support AST time at H_2/air and H_2 (3, 4, 5 %)/air
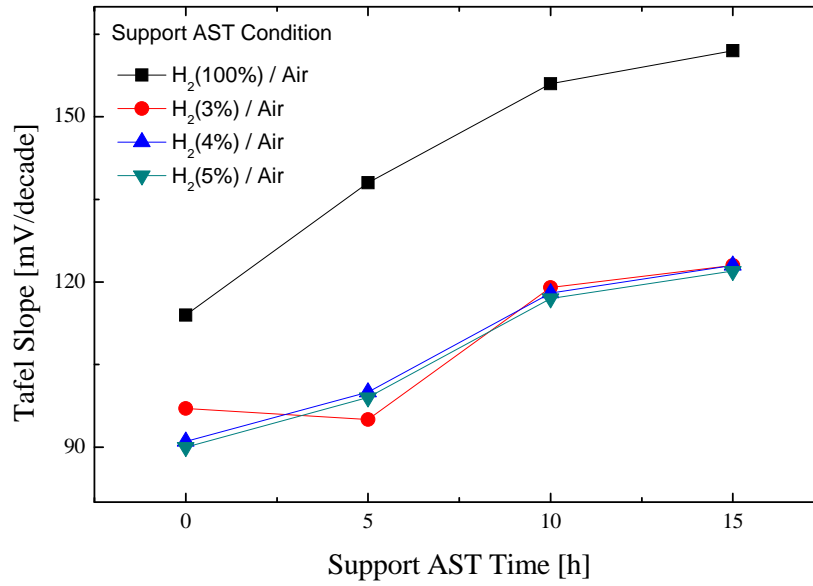
(b) Tafel slope against support AST time at H_2/air and H_2/O_2 (2, 4, 6 %)
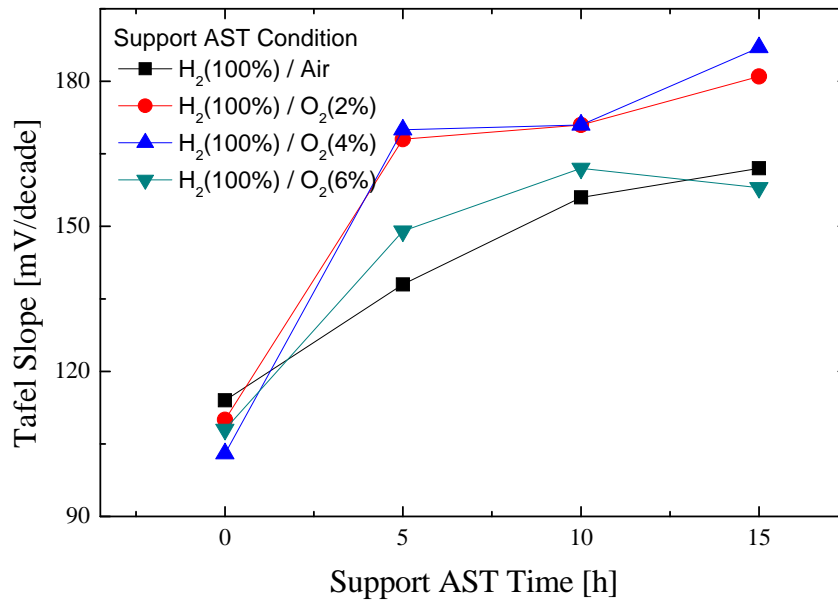
Figure 3.7 Tafel slope against support AST plotted with reactants of (a) H_2/air and H_2 3, 4, 5%/air and (b) H_2/air and H_2/O_2 2, 4, 6%.

(a) Activation overvoltage at H₂/air

(b) Activation overvoltage at hydrogen (H₂ 3, 4, 5%)/air

(c) Activation overvoltage at H₂/oxygen (O₂ 2, 4, 6%)
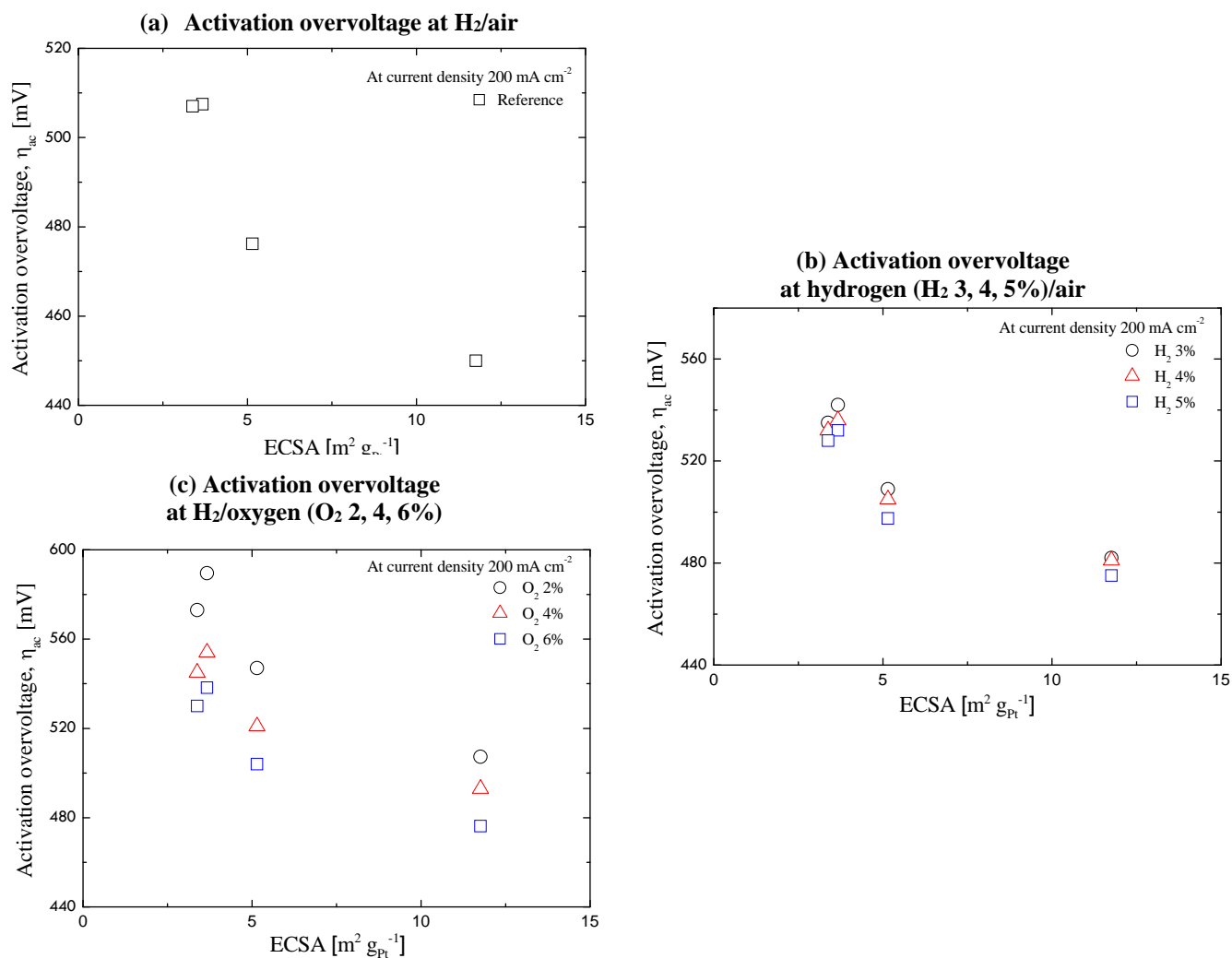
Figure 3.8 Activation overvoltages of H₂/air, H₂ (3, 4, 5%)/air and H₂/O₂ (2, 4, 6%) were indicated in (a), (b) and (c) respectively against ECSA under support AST. Each symbols in the figures represent activation overvoltage with each reactant concentration for condition of An 2 lpm/Ca 3 lpm, cell temperature of 65℃ and RH 100%.

Significant increase of contribution of mass transport overvoltage in figure 3.9 with above polarization curves indicate mass transport resistance increased at all feed conditions. With reduction of thickness of catalyst layer which acts as decrease of mass transport and the loss of catalyst increase the distance through ionomer and subsequent increase of contacts of ionomer. we could expect increase of contacts of ionomer and subsequent decrease of contribution of mass transport but limiting current density which shows state that kinetics of supply of reactant

dominate whole reaction kinetics were decreased. It means that contacts of ionomer will not be increased at least, which means that ionomer in CCL is also degraded. And mass transport resistance of oxygen may be increased because the loss of catalyst cause increase of distances that oxygen transport to Pt catalyst.

(a) Contribution of mass transport overvoltage at H₂/air
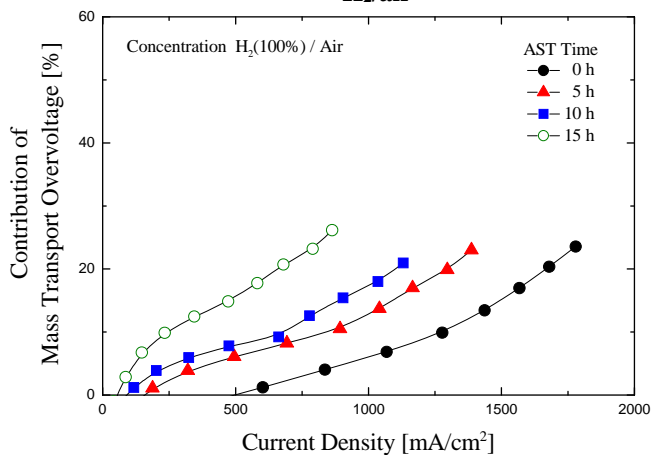
(b) Contribution of mass transport overvoltage at H₂ 4%/air
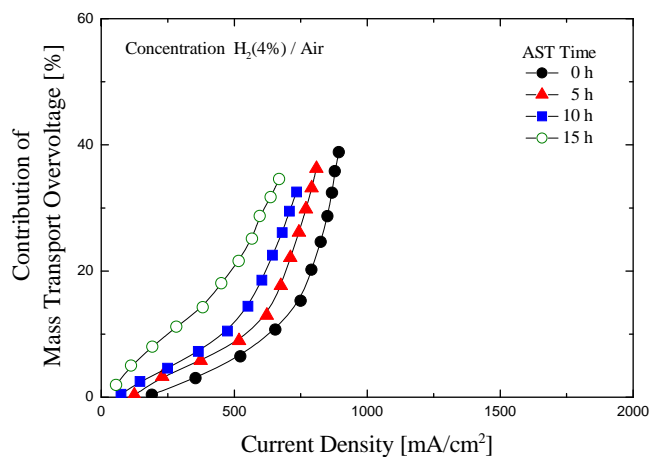
(c) Contribution of mass transport overvoltage at H₂/O₂ 4%
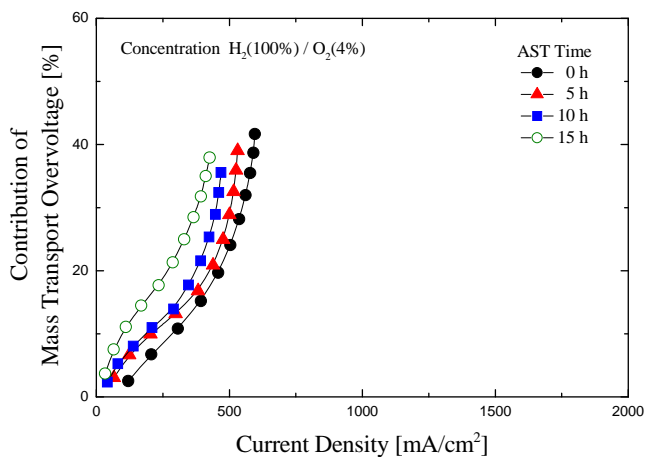
Figure 3.9 Contribution of mass transport overvoltages as a function of the current density with each symbols represent respectively states between 5 hour of support AST process at (a) H₂/air, (b) H₂ 4%/air and (c) H₂/O₂ 4% conditions of An 2 lpm/Ca 3 lpm, cell temperature of 65℃ and RH 100%.

To summarize results of experimental data, with carbon support loss after degradation oxygen

transport distance to the catalyst in CCL significantly increased. Contacts of carbon support and membrane/ionomer in CCL individually decreased. And local environment which surrounds carbon support changed. Following figure 3.10 shows the systematic analysis on the identifying cause of degradation under support AST.
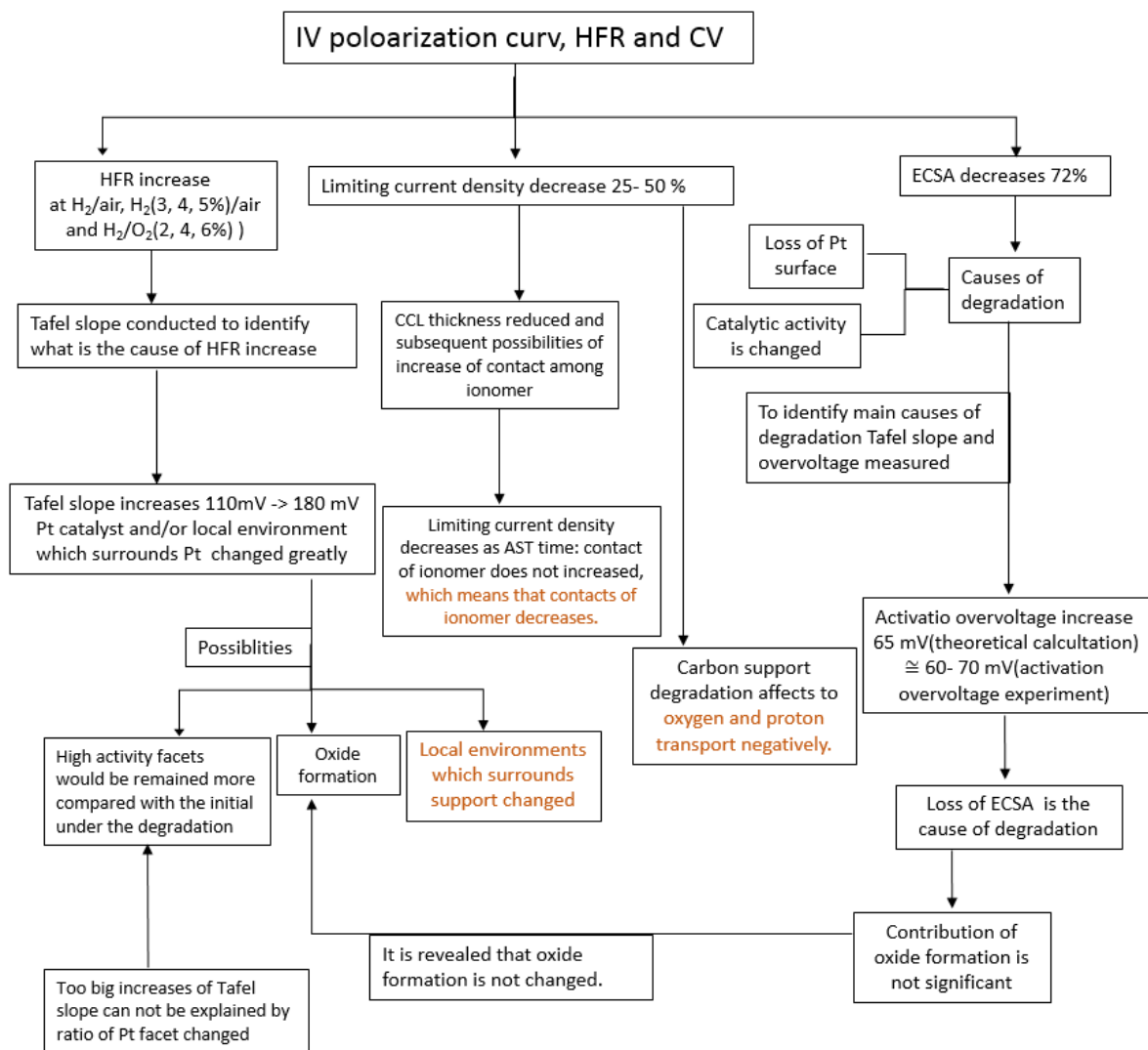
Figure 3.10 Systematic analysis scheme of degradation under AST on support materials.

3.3 Microstructural changes of MEA under AST on membrane/ionomer materials

Membrane/ionomer AST known as the process which mainly causes membrane/ionomer degradation was conducted with conditions of OCV hold (each set of 20 hours consists of three sets), cell temperature 90℃ and RH 10%. Membrane/ionomer degradation is not the successive progress but catastrophic progress[30-32]. This process usually accompanies cutting off of the chains of components of membrane/ionomer chemically and then formation of pinholes physically occur. And according to formation of pinholes in the membrane/ionomer in CCL hydrogen permeation current increased rapidly.

Polarization curve, HFR and CV were measured at H_2/air, H_2 (3, 4, 5 %)/air and H_2/O_2 (2, 4, 6 %) under the membrane/ionomer AST, and analysis of that are:

(1) HFR remained almost constant and indicates that almost no changes of contacts between carbon support and ionomer were exist.

(2) Losses of limiting current density in figure 3.11 were 8~18%, which were relatively small changes compared to carbon support AST.

(3) Pt ECSAs were reduced about 16% (after fully degraded, we cannot define the ECSA because of too much inclined CV shape). In addition, after 60 hours hydrogen permeation current also increased significantly about ten times. Increment of activation overvoltages in figure 3.12 were about 10 mV at H_2/air, H_2 (3, 4, 5 %)/air and H_2/O_2 (2, 4, 6 %). Almost no changes on Tafel slope also coincident with increment of activation overvoltage that Pt catalyst and local environment which surrounds the Pt catalyst may have not been changed.

Considering reduction of membrane and CCL thickness, it is expected that the distance which proton transport through catalyst layer is decreased and then it may cause limiting current

density increases but opposite experimental result may indicates that membrane and ionomer in CCL structure collapsed. Contribution of mass transport overvoltages at H_2 4%/air in figure 3.13 most increased within other cases. This result also sustain morphological collapse of membrane/ionomer as SEM analysis of reduction of thickness indicated. But rather contribution of mass transport overvoltages at H_2/air and H_2/O_2 4% were almost same as the initial and it means that oxygen mass transport were not affected by degradation.

We concluded that membrane/ionomer degradation causes the morphological collapse of membrane/ionomer and subsequent loss of proton transport occurs. Following figure 3.14 shows the systematic analysis on the identifying cause of degradation under membrane/ionomer AST.

(a) Polarization curves at H₂/air

(c) Polarization curves at H₂/O₂ 4%

(b) Polarization curves at H₂ 4%/air
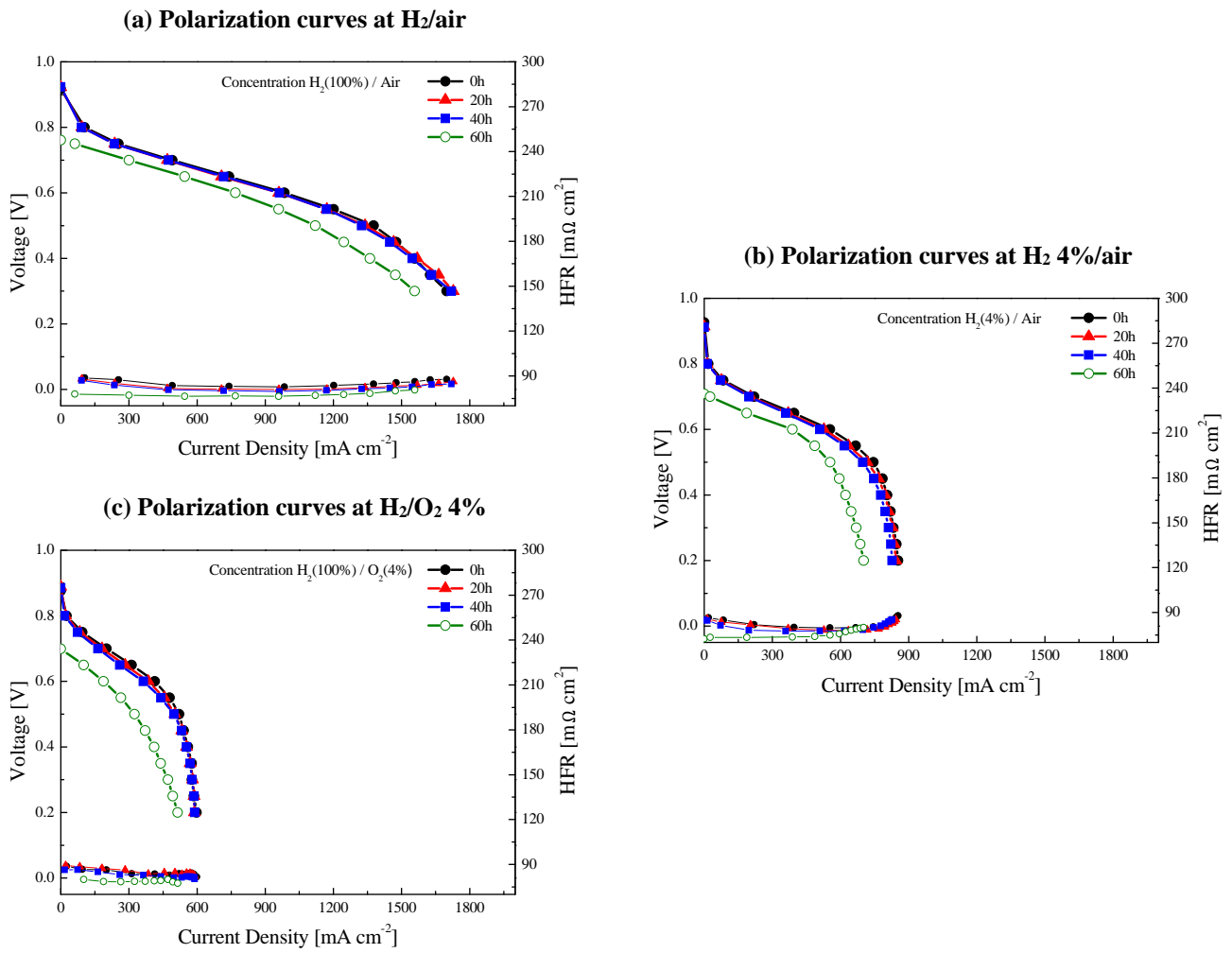
Figure 3.11 The polarization curve and HFR of H₂/air, H₂ 4%/air and H₂/O₂ 4% were indicated in (a), (b) and (c) respectively against current density under membrane/ionomer AST. Each lines in the figures represented polarization curve with each AST set of 20 hours for condition of An 2 lpm/Ca 3 lpm, cell temperature of 65℃ and RH 100%.

(a) Activation overvoltage at H₂/air

(b) Activation overvoltage at hydrogen(H₂ 3, 4, 5%)/air

(c) Activation overvoltage at H₂/oxygen (O₂ 2, 4, 6%)
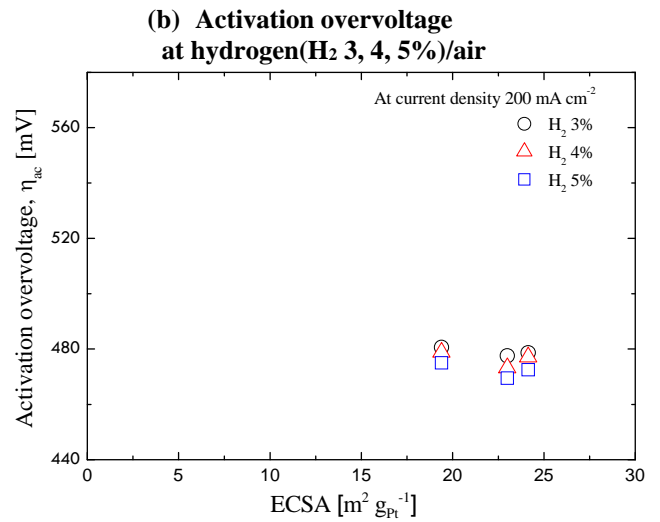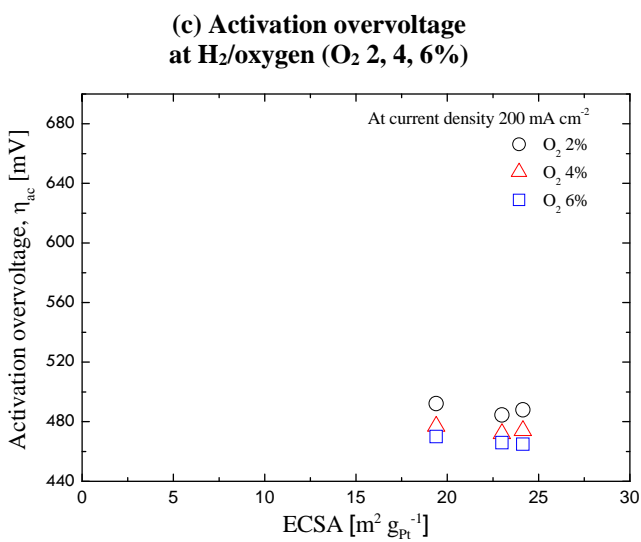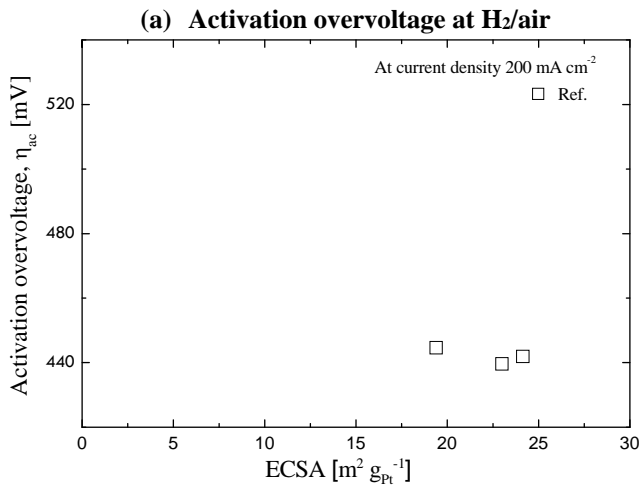
Figure 3.12 Activation overvoltages of H₂/air, H₂ 4%/air and H₂/O₂ 4% are indicated in (a), (b) and (c) respectively against ECSA under membrane/ionomer AST. Each points in the figures represent activation overvoltages with each cases for conditions of An 2 lpm/Ca 3 lpm, cell temperature of 65℃ and RH 100%.

(a) Contribution of mass transport overvoltage at H₂/air

(b) Contribution of mass transport overvoltage at H₂ 4%/air

(c) Contribution of mass transport overvoltage at H₂/O₂ 4%
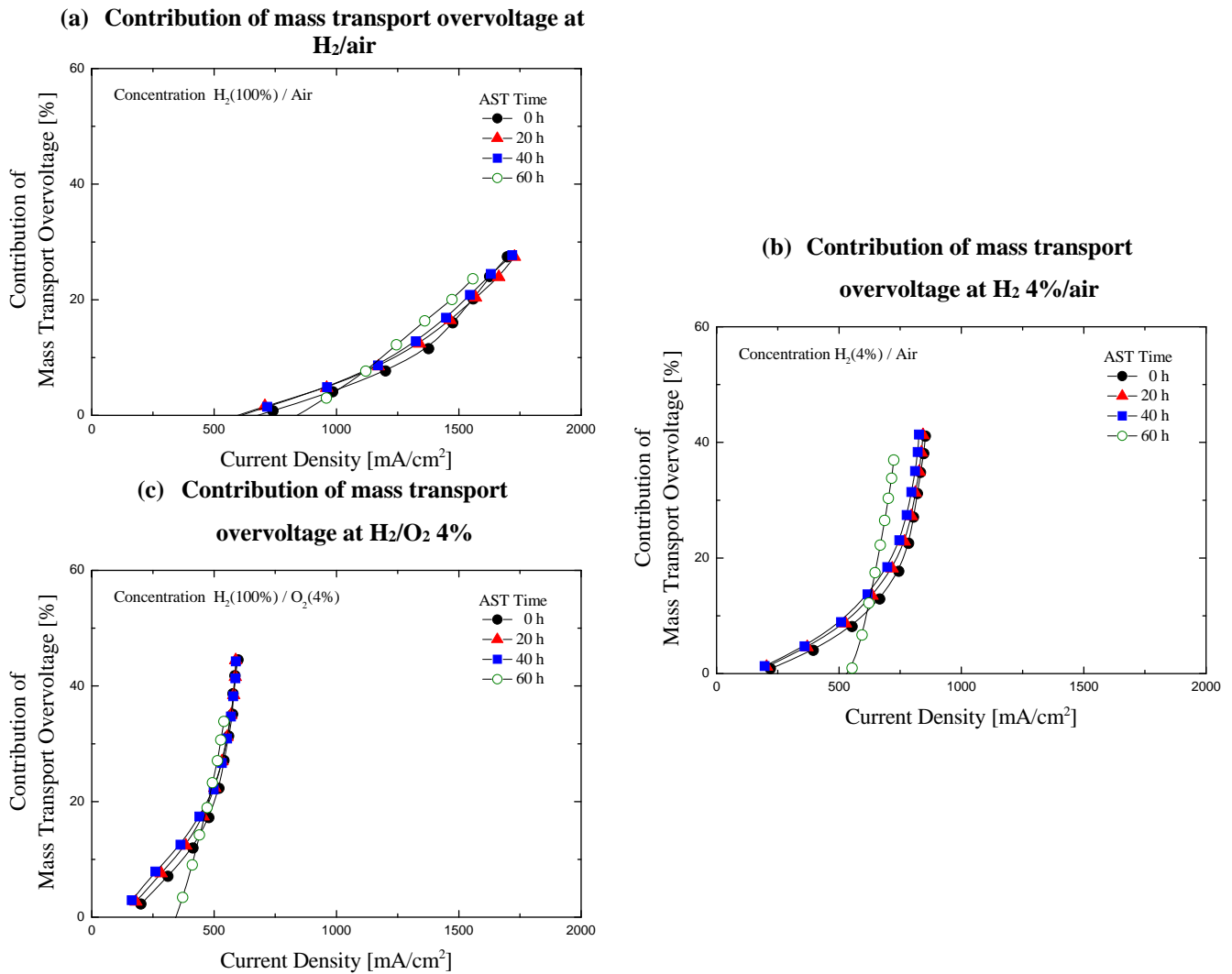
Figure 3.13 Contribution of diffusion overvoltages as a function of the current density with each lines represents respectively states between 20h membrane/ionomer AST process at (a) H₂/air, (b) H₂ 4%/air and (c) H₂/O₂ 4% conditions of An 2 lpm/Ca 3 lpm, cell temperature of 65℃ and RH 100%.

27
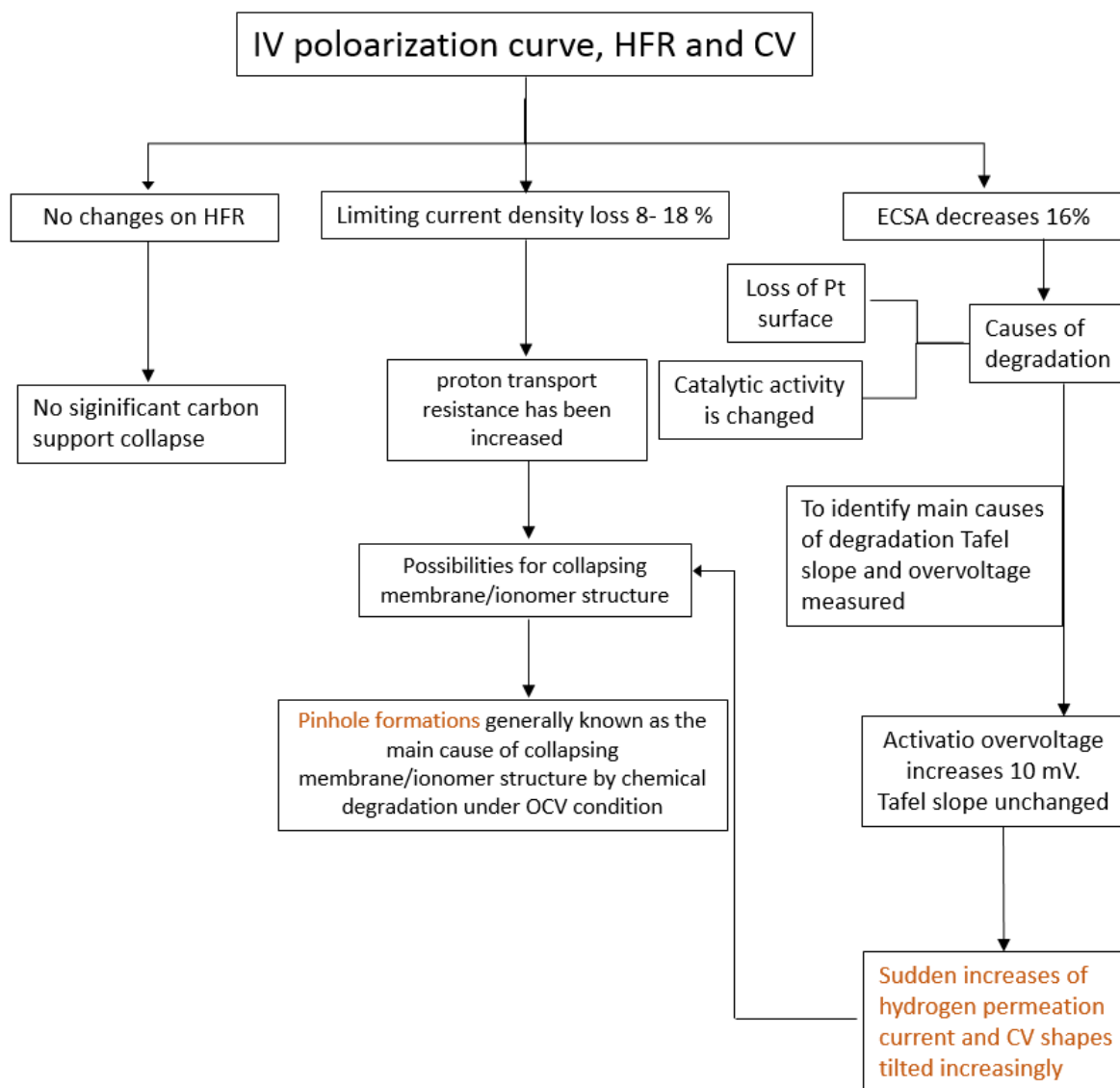
Figure 3.14 Systematic analysis scheme of degradation under AST on membrane/ionomer materials.

3.4 Integrated discussions

hitherto, we conducted various experiments to investigate the cause of degradation according to microstructural changes in MEAs and systematic analysis are done. Following figure 3.15 (a) – (d) shows cross-sectional thickness of MEAs by SEM images. From above in the figures cathode, membrane and anode are aligned. The mean thickness of the cathode and membrane

was calculated for each MEA from several individual micrographs. As shown at (a) - (c), there is no changes at membrane. But figure 3.15 (d) indicate serious thickness changes (about $8\mu m$ loss). The mean thickness of fresh cathode was estimated $9.82 \pm 0.28\mu m$, and that of after Support, Catalyst and membrane/ionomer degradation $4.92 \pm 0.44\mu m$, $7.12 \pm 0.68\mu m$ and $8.06 \pm 1.33\mu m$, respectively. Obviously changes of cathode indicates that AST process causes carbon support in CCLs corroded. Support AST has most significant changes at CCL thickness as providing the reduction of limiting current density. And membrane/ionomer AST has serious changes of membrane compared to other AST process. (support and catalyst AST does not affect membrane thickness).

The following table 4.1 show ECSA changes as AST time and it indicates that support and catalyst ECSA decrease decrease as AST time goes on but membrane/ionomer AST was significantly not affected by ECSA until 40 hours of AST and changes significantly as above result mentioned that membrane thickness reduced seriously.
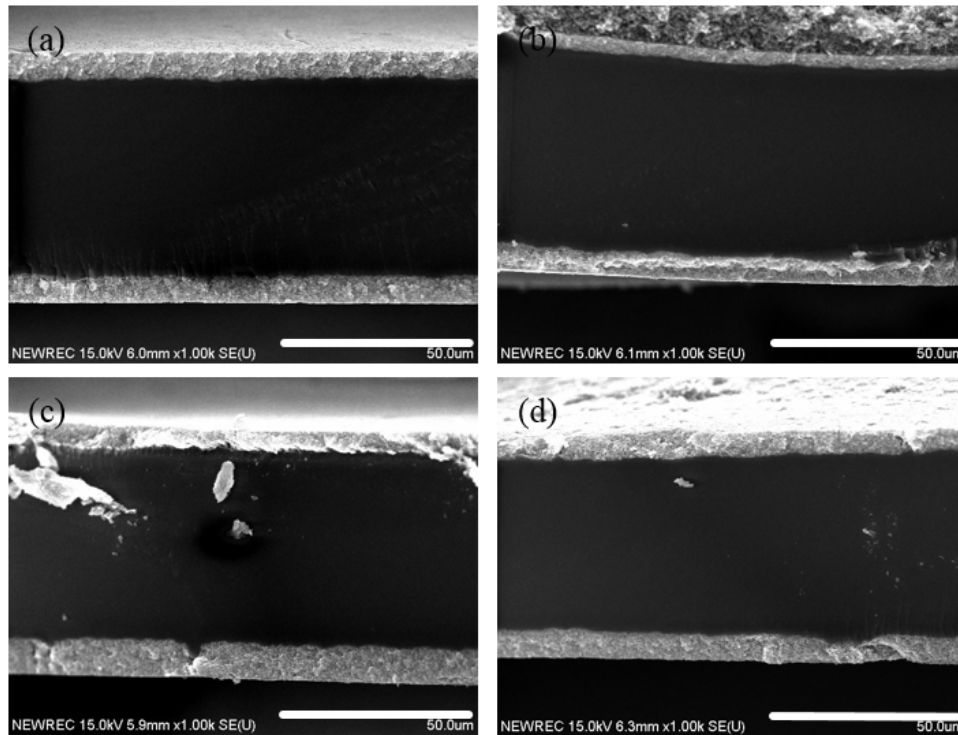
Figure 3.15 Cross-sectional SEM images: (a) the initial cross-section of MEA; (b) cross – section of MEA after 15 hours AST on support materials with 1.4 V voltage hold; (c) cross-section of MEA after 60000 cycles AST on catalyst materials with voltage sweep from 0.6 V to 1.0 V; (d) cross-section of MEA after 60 hours AST on membrane/ionomer AST on membrane/ionomer materials with OCV hold.

AST Number \ ECSA	Catalyst ECSA	Support ECSA	Membrane/ionomer ECSA
0	24.3	22.4	22.99
1	10.04	9.81	24.14
2	10.34	6.99	19.39
3	5.88	6.44	–

Table 4.1 Changes of ECSA with AST time

Following figure 3.16 show the normalized limiting current density and the changes of limiting current density directly show the changes of resistance of mass transport of reactants. As mentioned above, proton mass transport was not changed under the catalyst AST and oxygen mass transport was not changed as other AST procedure under the membrane/ionomer AST.
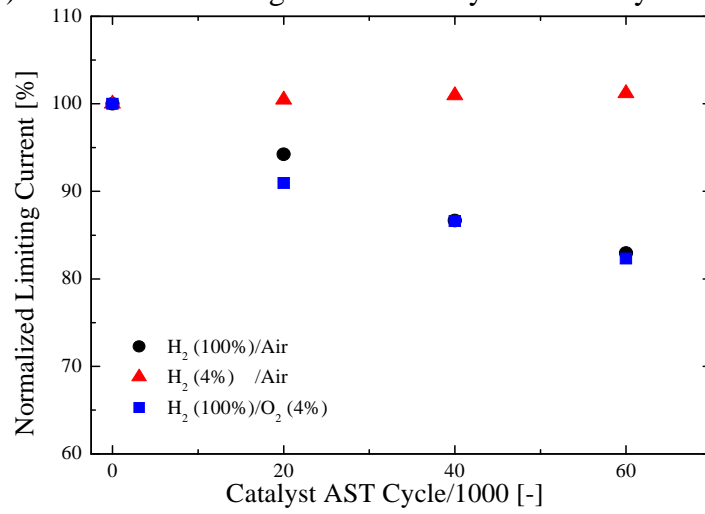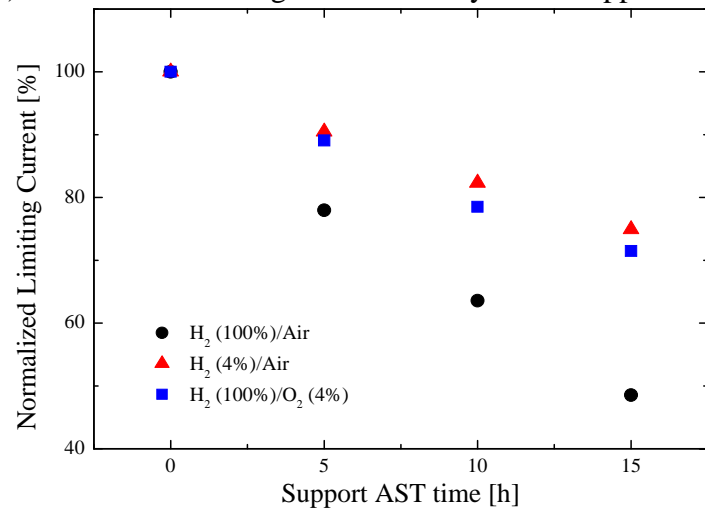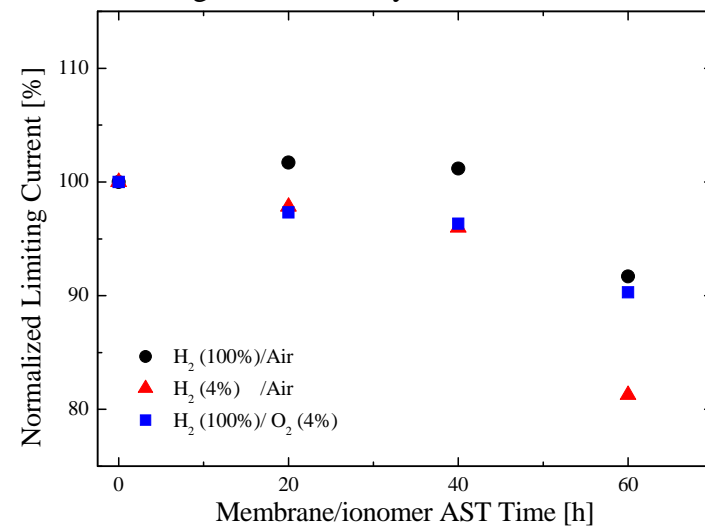
Figure 3.16 normalized limiting current against (a) each 20000 cycles of catalyst AST, (b) each 5 hours of support AST and (c) each 20 hours of membrane/ionomer AST.

Finally, as limiting current density indicates the mass transport, slope of current/gas concentration also shows the trends of mass transport of reactants.

Figure 3.17, slope of graph represents the likeness of mass transport which is proportional of inverse of mass transport resistance. At low concentration of hydrogen and oxygen conditions, all slope of limiting current/gas concentration decreased with AST time except the low oxygen concentration condition. And it means that mass transport resistance increased. Intercept of limiting current/gas concentration decreases as AST time and it indicates that CCL does not show homogeneous degradation rate.

(a) Slope of limiting current/Gas concentration at low H₂ concentration

(b) Intercept of limiting current/Gas concentration at low H₂ concentration

(c) Slope of limiting current/Gas concentration at low O₂ concentration

(d) Intercept of limiting current/Gas concentration at low O₂ concentration
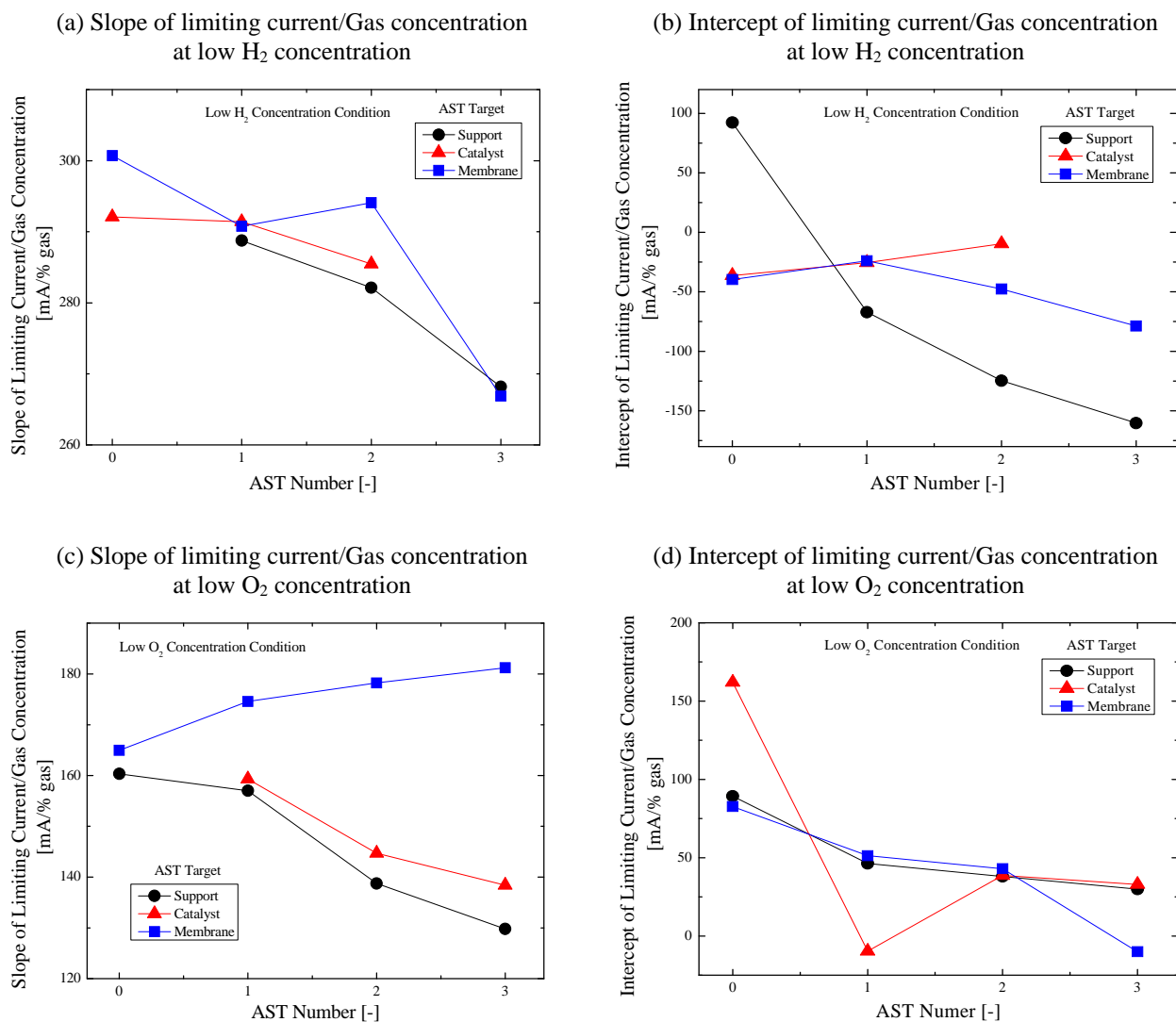
Figure 3. 17 Normalized limiting current/gas concentration against AST number. Slope of limiting current/gas concentration at low (a) H₂ concentration, (c) O₂ concentration and intercept of limiting current/gas concentration at low (b) H₂ concentration, (d) O₂ concentration have been shown. Black lines show the cases of support AST, red lines show the cases of catalyst and blue lines show the cases of membrane at all figures in each lines.

33

Chapter 4

Conclusions

This thesis estimates mechanisms and causes of degradation of PEMFC especially in MEA. The PEMFC consists Pt/C electrodes and single 1.5 cm^2 active area. ASTs have been conducted to apply specific real degradation situation in reasonably fast time. With AST time goes on, microstructures of MEA had been conducted by various in-situ electrochemical measurements and SEM which belongs to ex-situ measurement. Using these methods with H₂/air, H₂ (3, 4, 5%)/air and H₂/O₂ (2, 4, 6%) reactants, we could provide explanation of microstructures of CCL under three modes of AST because with low concentrated reactants, mass transport effects were extremely expressed.

We observe that catalyst AST cause Pt catalyst degraded significantly (about 75%) but higher catalytic activity of Pt facets remained more so performance loss had not been serious. Pt catalyst loss causes oxygen to lengthen the distance which it have to transported through catalyst layer and polarization curve at H₂/O₂ (2, 4, 6%) indicates oxygen transport resistance increased. Support AST cause most significant impact on deterioration of single cell performance and collapsing structures of CCL by affecting both carbon support and ionomer. Fully degraded support AST cause limiting current density drops from 1780 mA/cm^2 to 860 mA/cm^2 which is about 52% losses from initial state at H₂/air and most significant reduction of CCL thickness among three modes of AST. Briefly carbon support occurs at high voltage conditions and subsequent ionomer contacts loss and catalyst loss occurs. Oxygen transport distance increased according to Pt catalyst degradation and proton transport also hindered because of ionomer contacts loss. Membrane/ionomer AST shows morphological changes of microstructures of CCL, which is pinhole formation because OCV deterioration and extremely

increased hydrogen permeation current evidently indicate pinhole formation of cell in CCL. And SEM analysis indicate that loss of membrane thickness which was caused by OCV conditions. With increased contribution of mass transport overvoltages at low hydrogen concentration condition which is differ from the analysis that reduction of membrane thickness cause limiting current density of low hydrogen concentration increased and this means that collapse of membrane occurs. Moreover, rapidly increased hydrogen permeation current which may supports the idea of pinhole formation.

References

1   Tietenberg, T. H. & Lewis, L. *Environmental and natural resource economics*. (Addison-Wesley Reading, MA, 2000).

2   Schultz, M. G., Diehl, T., Brasseur, G. P. & Zittel, W. Air pollution and climate-forcing impacts of a global hydrogen economy. *Science* **302**, 624-627 (2003).

3   Dincer, I. Environmental and sustainability aspects of hydrogen and fuel cell systems. *International Journal of Energy Research* **31**, 29-55 (2007).

4   Hirschenhofer, J., Stauffer, D. & Engleman, R. Fuel cells: a handbook (Revision 3). (Gilbert/Commonwealth, Inc., Reading, PA (United States), 1994).

5   O'Hayre, R., Colella, W., Cha, S.-W. & Prinz, F. B. Fuel Cell Fundamentals.

6   Liu, Y.-H., Yi, B., Shao, Z.-G., Xing, D. & Zhang, H. Carbon Nanotubes Reinforced Nafion Composite Membrane for Fuel Cell Applications. *Electrochemical and Solid-State Letters* **9**, A356-A359, doi:10.1149/1.2203230 (2006).

7   Fernandes, A. C. & Ticianelli, E. A. A performance and degradation study of Nafion 212 membrane for proton exchange membrane fuel cells. *Journal of Power Sources* **193**, 547-554, doi:http://dx.doi.org/10.1016/j.jpowsour.2009.04.038 (2009).

8   Pei, P., Yuan, X., Chao, P. & Wang, X. Analysis on the PEM fuel cells after accelerated life experiment. *International Journal of Hydrogen Energy* **35**, 3147-3151, doi:http://dx.doi.org/10.1016/j.ijhydene.2009.09.103 (2010).

9   Yuan, X.-Z., Li, H., Zhang, S., Martin, J. & Wang, H. A review of polymer electrolyte membrane fuel cell durability test protocols. *Journal of Power Sources* **196**, 9107-9116, doi:http://dx.doi.org/10.1016/j.jpowsour.2011.07.082 (2011).

10   Zheng, C. H., Xu, G. Q., Park, Y. I., Lim, W. S. & Cha, S. W. Prolonging fuel cell stack lifetime based on Pontryagin's Minimum Principle in fuel cell hybrid vehicles and its economic influence evaluation. *Journal of Power Sources* **248**, 533-544, doi:http://dx.doi.org/10.1016/j.jpowsour.2013.09.110 (2014).

11   *http://energy.gov/sites/prod/files/2014/03/f9/fy15_at-a-glance_fcto.pdf*.

12   de Bruijn, F. A., Dam, V. A. T. & Janssen, G. J. M. Review: Durability and Degradation Issues of PEM Fuel Cell Components. *Fuel Cells* **8**, 3-22, doi:10.1002/fuce.200700053 (2008).

13   Wu, J. *et al.* A review of PEM fuel cell durability: degradation mechanisms and mitigation strategies. *Journal of Power Sources* **184**, 104-119 (2008).

14   Borup, R. *et al.* Scientific aspects of polymer electrolyte fuel cell durability and degradation. *Chemical reviews* **107**, 3904-3951 (2007).

15   Larminie, J., Dicks, A. & McDonald, M. S. *Fuel cell systems explained*. Vol. 2 (Wiley New York, 2003).

16   Sun, W., Peppley, B. A. & Karan, K. An improved two-dimensional agglomerate cathode model to study the influence of catalyst layer structural parameters. *Electrochimica Acta* **50**,

3359-3374 (2005).

17   Mukherjee, P. P. & Wang, C.-Y. Direct numerical simulation modeling of bilayer cathode catalyst layers in polymer electrolyte fuel cells. *Journal of The Electrochemical Society* **154**, B1121-B1131 (2007).

18   Secanell, M., Carnes, B., Suleman, A. & Djilali, N. Numerical optimization of proton exchange membrane fuel cell cathodes. *Electrochimica Acta* **52**, 2668-2682 (2007).

19   knights, S. *4th Annual International Fuel Cell Testing Workshop* **Vancouver, BC, Canada** (2007).

20   Oyarce, A. *et al.* Comparing shut-down strategies for proton exchange membrane fuel cells. *Journal of Power Sources* **254**, 232-240 (2014).

21   Siegel, N. P., Ellis, M. W., Nelson, D. J. & von Spakovsky, M. R. Single domain PEMFC model based on agglomerate catalyst geometry. *Journal of Power Sources* **115**, 81-89, doi:10.1016/s0378-7753(02)00622-5 (2003).

22   Zhang, S. *et al.* A review of accelerated stress tests of MEA durability in PEM fuel cells. *International Journal of Hydrogen Energy* **34**, 388-404 (2009).

23   Eastwood, B., Christensen, P., Armstrong, R. & Bates, N. Electrochemical oxidation of a carbon black loaded polymer electrode in aqueous electrolytes. *Journal of Solid State Electrochemistry* **3**, 179-186 (1999).

24   Cai, M. *et al.* Investigation of thermal and electrochemical degradation of fuel cell catalysts. *Journal of Power Sources* **160**, 977-986 (2006).

25   Gasteiger, H. A., Kocha, S. S., Sompalli, B. & Wagner, F. T. Activity benchmarks and requirements for Pt, Pt-alloy, and non-Pt oxygen reduction catalysts for PEMFCs. *Applied Catalysis B: Environmental* **56**, 9-35 (2005).

26   Macia, M., Campina, J., Herrero, E. & Feliu, J. On the kinetics of oxygen reduction on platinum stepped surfaces in acidic media. *Journal of Electroanalytical Chemistry* **564**, 141-150 (2004).

27   Park, S. *et al.* Degradation of the Ionic Pathway in a PEM Fuel Cell Cathode. *The Journal of Physical Chemistry C* **115**, 22633-22639, doi:10.1021/jp2068599 (2011).

28   Shao-Horn, Y. *et al.* Instability of supported platinum nanoparticles in low-temperature fuel cells. *Topics in Catalysis* **46**, 285-305 (2007).

29   Merzougui, B. & Swathirajan, S. Rotating Disk Electrode Investigations of Fuel Cell Catalyst Degradation Due to Potential Cycling in Acid Electrolyte. *Journal of the Electrochemical Society* **153**, A2220, doi:10.1149/1.2353752 (2006).

30   Yu, J., Matsuura, T., Yoshikawa, Y., Islam, M. N. & Hori, M. In situ analysis of performance degradation of a PEMFC under nonsaturated humidification. *Electrochemical and Solid-State Letters* **8**, A156-A158 (2005).

31   Schmittinger, W. & Vahidi, A. A review of the main parameters influencing long-term performance and durability of PEM fuel cells. *Journal of Power Sources* **180**, 1-14,

doi:http://dx.doi.org/10.1016/j.jpowsour.2008.01.070 (2008).

32   Patil, Y. P., Jarrett, W. L. & Mauritz, K. A. Deterioration of mechanical properties: A cause for fuel cell membrane failure. *Journal of Membrane Science* **356**, 7-13, doi:http://dx.doi.org/10.1016/j.memsci.2010.02.060 (2010).

국문요약

**가속스트레스시험 방법을 이용한
고분자전해질 연료전지의 열화 기작에 관한 실험적 연구**

　고효율의 녹색 에너지인 연료전지는 내구성의 문제로 특히 연료전지 자동차의 상용화에 어려움을 겪고 있다. 또한 내구성에 관한 연구가 계속 진행되고 있지만 여전히 단편적인 열화 기작들만 제시되어 왔다. 본 연구에서는 전기화학적 방법들과 전자주사현미경 측정을 통해 가속스트레스시험이 진행됨에 따른 막전극접합체의 미세구조 변화를 평가하였다. 그리고 그에 따른 열화의 각 요소들을 검증해 나가면서 열화기작과 열화의 요인들을 체계적으로 분석하였다. 본 연구를 수행하기 위해서 먼저 막전극접합체를 제작하고 셀의 다른 요소들을 준비하여 실험 시스템을 꾸몄으며 주로 열화시키는 셀의 요소들이 서로 다른 세가지 종류의 가속스트레스시험 방법을 통하여 충분히 빠른 시간 안에 실제의 상황을 재현해보려 하였다. 분극곡선과 고주파저항 그리고 순환전압전류법을 통하여 셀의 열화경향성과 각 셀의 요소들간의 연결도 그리고 전기화학적 활성 비표면적의 변화를 살펴보았고 타펠 기울기와 활성화 과전압을 통하여 백금입자의 성질에 대한 해석을 가능케 하였다. 한계 전류밀도와 반응물의 공급의 저항에 대한 기여도는 반응물의 공급 정도를 직관적으로 알 수 있게 해 준다. 이를 통해서 본 실험에서는 탄소 지지체의 무너짐과 그에 따른 환경의 변화가 탄소 지지체 물질에 대한 가속스트레스시험 에서의 열화에 대한 주요인이며, 아이오노머와 지지체의 연결도와 촉매의 열화가 동시에 촉매 물질 열화에 대한 가속스트레스시험 에서의 열화에 대한 주요인이며 막 및 아이오노머에 대한 가속스트레스시험 에서는 핀홀의 형성이 열화에 대한 주요인인 것을 알 수 있었다.

핵심어: 가속스트레스시험, 한계전류밀도, 열화, 내구성,고분자전해질 연료전지

Acknowledgement (감사의 글)

"네 틀을 깨지 않으면 넌 앞으로 계속 같은 실패를 할 수 밖에 없다. 그리고 그 틀은 누가 깨어 주지 않는다" 지도 교수님인 한병찬 교수님께서 진지하게 학문과 삶에 대해서 해 주신 충고 중 가장 많이 뇌리에 와 닿은 말씀이었습니다. 비록 실천하기 까지 많은 시간과 망설임과 어려움이 많았지만 그러한 충고를 들을 수 있는 기회를 주시고 한 걸음 뗄 수 있도록 때론 엄한 질책으로 때론 본질을 파고드는 질문으로 사랑의 격려를 해 주신 한병찬 교수님께 진심으로 감사합니다. 그리고 석사 과정 중 11개월의 파견 생활에서 저 스스로를 돌아볼 수 있게 해 주셨고 실제적인 연구자로서, 공학자로서의 모습을 보여 주시고 가르쳐 주신 공동 논문 지도 교수님이신 한국에너지기술연구원의 윤영기 박사님께도 진심으로 감사합니다. Sangaraju Shanmugam 교수님께도 조언을 아끼지 않아 주심을 감사 드립니다.

학위 과정 중 많은 도움을 주신 서민호 박사님, 준교형, 승효형, 인혜누나, 동기로 들어온 준희와 혜림, 인턴으로 와 있던 기돈 형과 abhishek, 후배인 도현, 주승, 혜진, 수연 모두 에게 말할 수 없는 도움과 격려와 사랑을 받았음을 고백합니다.

한국에너지기술연구원 부안센터에서 부족한 절 품어 주셨던 이은재 과장님, 최영우 박사님, 김태영 박사님 그리고 실험적 기술을 도와 주고 물심양면으로 도와주셨던 김성완 선생님, 이미순 선생님, 지일형, 민호형, 용민형, 현구형, 찬희형, 용형, 동준, 지성, 다영, 원재, 승용 모두에게 감사의 인사를 전합니다.

경북대학교에서 이론 물리를 연구하시던 안창현 교수님과 우경성 박사님께도 학문에 흥미를 가질 수 있도록 풍부한 지식과 조언으로 늘 도와 주시고 격려하여 주심을 감사합니다.

아울러 이 석사 과정 중에 많이 격려해 준 함성호 교수님, 기독센터 사생 동기들, 선후배들에게 특별히 심심한 감사의 뜻을 전합니다. 그리고 힘들 때마다 마음의 기초를 다시 쌓을 수 있는 믿음의 말씀으로 도전을 준 별이 아빠 김민 형님께도 감사 드립니다. 저를 위해서 기도해 주신 분들께도 감사 드립니다.

그리고 누구보다 진심으로 걱정해 주시고 위로해 주시고 격려해 주시던 할머니, 아버지, 어머니, 동생 선영이에게 깊은 사랑과 감사의 뜻을 전합니다.

마지막으로 아직 부족하고 미약하며 미련하여 넘어지는 어린아이의 신앙이지만 2년 반 동안의 석사 과정을 무사히 마치게 해 주시고 그 과정 중 저에게 맞는 훈련 과정을 거치게 하시고 깨닫게 하신 하나님께 무한한 사랑과 감사의 뜻을 표현합니다. 외모를 보지 않으시고 오직 중심을 보시는 하나님께 더욱더 나아가 앞으로의 삶에서 첫사랑을 찾으며 '그러므로 하늘에 계신 너희 아버지의 온전하심과 같이 너희도 온전하라' (마태복음 5:48) 하신 말씀을 이루실 주님을 찬양합니다.

Curriculum Vitae

Name: Sangheum Byun

Birth Date: 1987.02.26

Education

2006-2012 B.S., Department of Energy Sciences, Kyungpook National University

2012-2014 M.S., Department of Energy Systems Engineering, DGIST